2005

U-Pb Zircon Ages and Pb Isotope Geochemistry of Gold Deposits in the Carolina Slate Belt of South Carolina

R. A. Ayuso
U.S. Geological Survey, Mail Stop 954, National Center, Reston, Virginia 20192

J. L. Wooden
U.S. Geological Survey, Stanford-U.S. Geological Survey Micro-Isotopic Analytical Center (SUMAC), Stanford University, Stanford, California 94305-2220

N. K. Foley
U.S. Geological Survey, Mail Stop 954, National Center, Reston, Virginia 20192

Robert R. Seal II
U.S. Geological Survey, 954 National Center, Reston, Virginia 20192, USA, rseal@usgs.gov

A. K. Sinha
Virginia Polytechnic Institute and State University

©2005 Society of Economic Geologists, Inc.
Economic Geology, v. 100, pp. 225–252

U-Pb Zircon Ages and Pb Isotope Geochemistry of Gold Deposits in the Carolina Slate Belt of South Carolina

R. A. Ayuso,†
U.S. Geological Survey, Mail Stop 954, National Center, Reston, Virginia 20192

J. L. Wooden,
U.S. Geological Survey, Stanford-U.S. Geological Survey Micro-Isotopic Analytical Center (SUMAC), Stanford University, Stanford, California 94305-2220

N. K. Foley, R. R. Seal, II,
U.S. Geological Survey, Mail Stop 954, National Center, Reston, Virginia 20192

and A. K. Sinha
Department of Geological Sciences, Virginia Polytechnic Institute and State University, Blacksburg, Virginia 24010

Abstract

Volcanic rocks of the Persimmon Fork Formation host the largest known gold mines of the Carolina slate belt. U-Pb (SHRIMP) zircon ages have been obtained from rocks closely associated with pyrite-enargite-gold deposits at Brewer (quartz-topaz rhyolite breccia from the argillic alteration zone in the Brewer pit and felsic ash-flow tuff from the quartz sericite alteration zone), from the disseminated and semimassive pyrite-gold deposits at Haile (crystal lithic rhyolitic ash-flow tuffs from the Champion pit), and from the Ridgeway deposit (felsic ash-flow tuff from the stratigraphic host of the North pit gold deposit). Generally, the zircons are fine grained, fractured, and contain crystal imperfections (corrosion, inclusions, and pits). $^{206}Pb/^{238}U$ zircon spot ages for all deposits span a wide range, mostly from 400 to 760 Ma. Inclusions and cores indicative of inherited domains in the zircons were not found, and only a few analyses range from 1.1 to 1.8 Ga. A distinct xenocrystic zircon population was not identified. The $^{206}Pb/^{238}U$ weighted age averages of zircon indicate the following crystallization dates for the volcanic and volcaniclastic rocks closely associated with the gold deposits: 550 ± 3 Ma for Brewer, 553 ± 2 Ma for Haile, and 556 ± 2 Ma for the Ridgeway deposit. These zircon crystallization ages represent close estimates of the age of the original gold mineralizing events. Younger zircon spot ages can be attributed to the effects of Paleozoic regional metamorphism.

Pb isotope compositions of sulfide minerals (galena, pyrite, enargite, sphalerite, chalcopyrite, and molybdenite) and silicate minerals (K-feldspar, and sericite) in the gold deposits help to constrain the sources of fluids and metals during the mineralizing events. The deposits are pyrite rich, containing multiple generations of pyrite, including early-crystallized pyrite that is closely associated with the original gold mineralizing event, as well as recrystallized pyrite formed in response to Paleozoic metamorphism. Pb isotope compositions of pyrite span a wide range, including the most radiogenic values for the sulfides. Galena and K-feldspar are not abundant but where present they are typically the least radiogenic minerals. Galena has a limited range of Pb isotope compositions that are representative of the gold deposits as a group ($^{206}Pb/^{204}Pb$ = 18.020–18.326, $^{207}Pb/^{204}Pb$ = 15.550–15.639, $^{208}Pb/^{204}Pb$ = 37.605–38.286). Values of $^{207}Pb/^{204}Pb$ straddle the average crustal Pb growth curve, consistent with contributions involving the mantle and continental crust. Whole-rock Pb isotope compositions of volcanic and volcaniclastic rocks of the Persimmon Fork Formation nearly match the range for sulfides in the gold deposits. Subtle regional contrasts in Pb isotope compositions exist among the deposits. Sulfide minerals from Barite Hill (e.g., galena $^{206}Pb/^{204}Pb < 18.077$) in southern South Carolina are generally less radiogenic than sulfides from Ridgeway ($^{206}Pb/^{204}Pb > 18.169$), Haile ($^{206}Pb/^{204}Pb > 18.233$), and Brewer ($^{206}Pb/^{204}Pb > 18.311$) in northern South Carolina. Because Pb isotope compositions of basement rocks from Grenville massifs in the southern Appalachians and sulfide minerals from the gold deposits do not match, a direct genetic connection cannot be established. Diversity in values of $^{206}Pb/^{204}Pb$ and the relatively high values of $^{207}Pb/^{204}Pb$ suggest that the deposits evolved adjacent to or closely related to continental blocks, perhaps linked to a back-arc tectonic setting. Among potential younger analogues of the slate belt gold deposits are the sulfide deposits of the Okinawa trough in the western Pacific. Mantle-derived isotopic contributions were more important at Barite Hill in southern South Carolina, the least radiogenic among the deposits where oceanic crust had developed, than at Brewer, Haile, and Ridgeway in northern South Carolina where rifting thinned the continental crust.

Introduction

The Carolina slate belt hosts numerous base metal and gold occurrences and several large volume and low-grade pyrite-rich gold deposits (Feiss and Slack, 1989). The slate belt extends from Georgia to Virginia and is part of the Carolina terrane (Fig. 1), which constitutes a portion of the Carolina zone (e.g., Secor et al., 1983; Horton et al., 1989). The Carolina zone consists of a sequence of Late Proterozoic to Early Paleozoic

† Corresponding author: e-mail, rayuso@usgs.gov

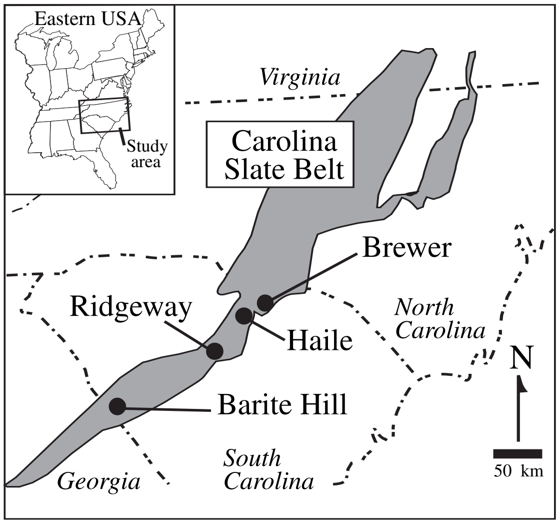

FIG. 1. A. Sketch map showing the Carolina slate belt (after Horton et al., 1989) and location of the major gold deposits in South Carolina: Brewer, Haile, Ridgeway, and Barite Hill.

metaigneous and metasedimentary rocks (e.g., Butler and Secor, 1991; Hibbard and Samson, 1995).

Gold deposits associated with hydrothermal magmatic systems and similar to those in the slate belt are distributed throughout portions of eastern North America northward to Maritime Canada (O'Brien et al., 2001). All of these are hosted by rocks that share a geologic affinity to the classic Avalonian tectonic zone (e.g., Williams and Hatcher, 1982), emphasizing the importance of this zone as a highly prospective region for gold deposits of this type (Huard and O'-Driscoll, 1986; Dubé et al., 1998; O'Brien et al., 1998, 2001, and references therein).

This study focuses on the U-Pb zircon geochronology and Pb isotope evolution of the three largest gold deposits in the Southern Appalachians of northern South Carolina (Fig. 1). From north to south, they are the Brewer (Fig. 2), Haile (Fig. 3), and Ridgeway (Fig. 4) deposits. We also report Pb isotope data for Barite Hill (Fig. 5), a gold-silver volcanogenic massive sulfide deposit near the South Carolina-Georgia border (Fig. 1). Gold exploration in the Southern Appalachians began more than 200 years ago, and small-scale mining is

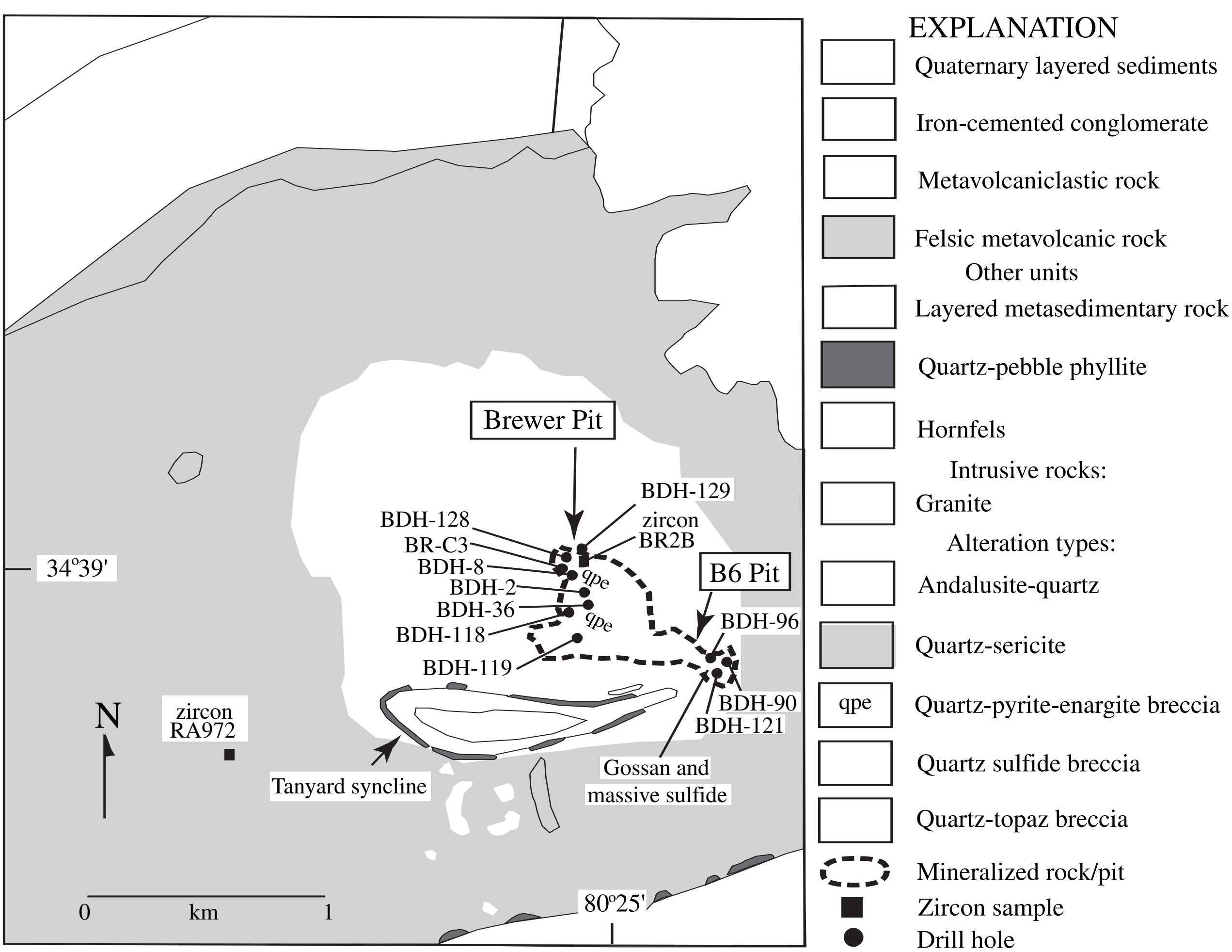

FIG. 2. Generalized geologic map of the Brewer gold deposit showing geologic units and alteration types (modified from Sheetz, 1991; Zwaschka and Scheetz, 1995), as well as drill hole and zircon sample locations. Quartz topaz breccia is found around samples BDH-128, BDH-129, and zircon sample BR-2B. Zircon sample RA972 was obtained about 1.5 km west of the Brewer pit in felsic metavolcanic rocks (N 34° 38.06, W 80° 26.34).

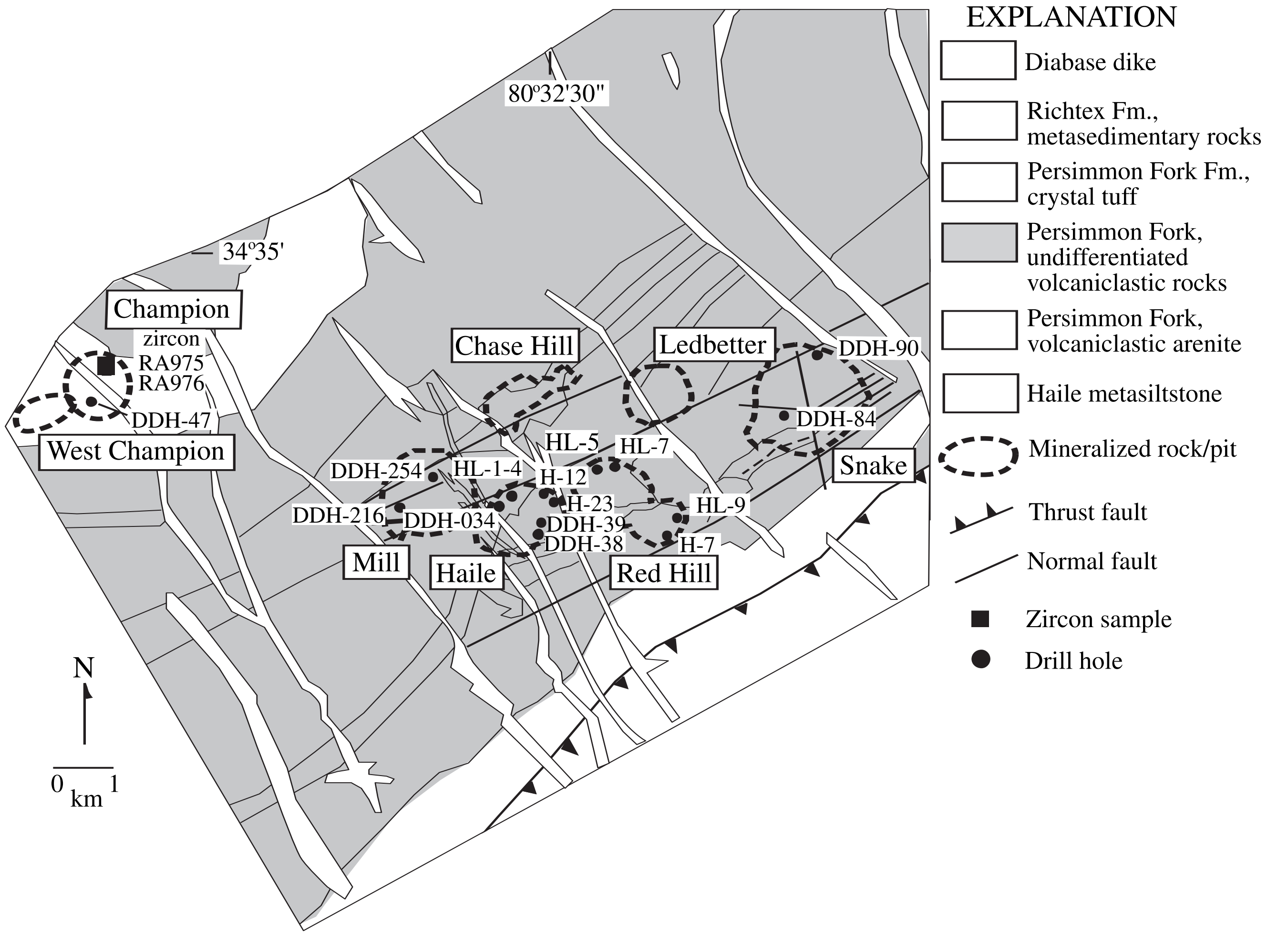

FIG. 3. Generalized geologic map of the Haile gold deposit showing geologic units and pits (from Maddry and Kilbey, 1995), as well as drill hole and zircon sample locations.

recorded as early as the 1820s at the Haile and Brewer mines (Worthington, 1993). The gold deposits in the slate belt remained in production until the 1990s. Tonnage and gold grade range from 5.6 mt, 1.2 g/t Au at Brewer (Zwaschka and Scheetz, 1995), 15.3 mt, 3.0 g/t Au at Haile (Maddry and Kilbey, 1995), 56 mt, 1.1 g/t Au at Ridgeway (Gillon et al., 1995, 1998), and 1.5 mt, 1.3 g/t Au at Barite Hill (D.J. LaPoint and C.H. Cherrywell, 1995, unpub. rept.).

Great progress has been made explaining the geologic evolution of the gold deposits, but their genesis is still a subject of debate (Worthington, 1993). Important aspects concerning the age of mineralization, metal and fluid sources, and tectonic settings remain unresolved. Numerical ages for the host volcanic rocks generally do not exist, and the exact timing of the mineralization has not been ascertained, although it is widely thought to be Neoproterozoic (e.g., Maddry and Kilbey, 1995; Stein et al., 1997; Gillon et al., 1998). The deposits were long considered to be granite-related hydrothermal quartz veins (Pardee and Park, 1948) until a volcanogenic (syngenetic, marine exhalative) origin was suggested (e.g., Worthington and Kiff, 1970; Spence et al., 1980; Kiff and Spence, 1987). In the 1990s, exploration models involving structural control (replacement and shear zone-related), gold remobilization, and hydrothermal fluids of metamorphic origin were prominent on the basis of work at the Haile (Tomkinson, 1988; Hayward, 1992) and Ridgeway deposits (Duckett et al., 1988; Gillon et al., 1995). The Ridgeway deposit has been related to an intra-arc basin (Gillon et al, 1998), in agreement with results of regional oxygen isotope variations of volcanic rocks that point to an evolving rift setting (Feiss et al., 1993). In this view, as intra-arc rifting progressed from subaerial to shallow submarine, the Brewer, Haile, and Ridgeway deposits were produced, followed by submarine Kuroko-type massive sulfide deposits (Barite Hill; Feiss et al., 1993).

In recent years we have studied various aspects of the gold deposits to contribute to the debate about their origin (e.g., Offield, 1994; Ayuso et al., 1997; Clark et al., 1999; Foley et al., 1997, 2001; Seal et al., 2001). This paper presents results of our U-Pb zircon geochronology study that was focused on the volcanic and volcaniclastic rocks hosting the gold deposits. New Pb isotope data also offer insights into the age of mineralization, mechanisms for metal transport, and regional comparisons (e.g., Richards and Noble, 1998).

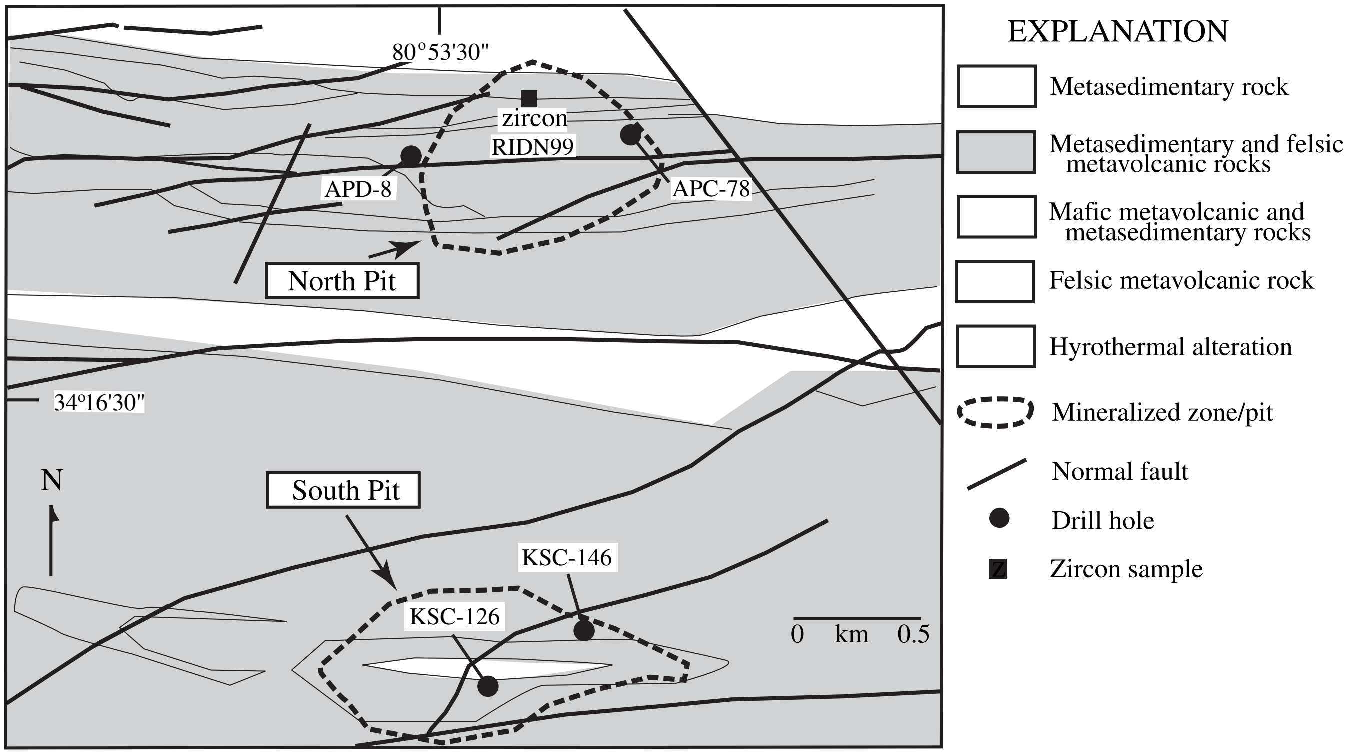

FIG. 4. Generalized geologic map of the Ridgeway gold deposit showing geologic units, pits, (from Gillon et al., 1998), and drill hole and zircon sample locations.

Geology of the Gold Deposits in the South Carolina Slate Belt

The major gold deposits occur adjacent to the contact between Late Neoproterozoic, intermediate to felsic pyroclastic rocks and overlying turbidites, graywackes, and epiclastic metasedimentary rocks (e.g., Worthington and Kiff, 1970). The Persimmon Fork Formation, part of a thick sequence of crystal and lapilli felsic tuffs and tuff breccias and minor basaltic rocks (Dennis, 1995), is the predominant host of the gold deposits, particularly where the volcanic rocks are interlayered with metasedimentary rocks. The Persimmon Fork Formation contains calc-alkaline ash flows (e.g., Whitney et al., 1978; Feiss, 1982; Dennis, 1995; Shervais et al., 1996). Mudstones, turbiditic wackes, and clastic-rich metasedimentary rocks that overlie the Persimmon Fork Formation belong to the Richtex Formation, which marks the transition from felsic- to mafic-dominated submarine volcanism, and from mudstones to turbiditic clastic sedimentation that accumulated in an intra-arc basin during rifting (Dennis and Shervais, 1996).

The slate belt deposits as a group can be characterized as pyritic-gold deposits and belonging to a class of gold-rich volcanic-associated massive sulfide deposits (e.g., Hannington et al., 1999, and references therein). Detailed evaluation of mineralization styles remains controversial, in part due to diverse features found within individual deposits, difficulties in properly assessing textural information, and deformation and metamorphic overprints on the fine-grained volcanic, volcaniclastic, and juvenile sedimentary rocks. Even within individual deposits there is wide variability in styles of mineralization that can include features diagnostic of volcanic-related deposits (e.g., auriferous colloform Fe sulfide and chemical sediments in layered tuffs and stockwork veining), sedimentary deposits (pyrite cubes in graded beds in mudstones), and metamorphic deposits (pyrite and gold remobilized in fold noses). The semimassive to disseminated style of low-sulfidation pyrite-gold mineralization at Haile (and Ridgeway) has been suggested as an example of intrusion-related, noncarbonate, stockwork mineralization (as defined by Sillitoe, 1991; Robert et al., 1997) in comparison with potentially coeval deposits in the Avalonian belt (Dubé et al., 1998; O'Brien et al., 1998, 2001). Notably, however, the Haile deposit also displays features typical of both hot spring-type pyrite-gold mineralization and stockwork-type mineralization in volcanic and volcaniclastic rocks and in breccia pipes, and remobilized and folded pyrite-gold quartz veins (Speer and Maddry, 1993; Maddry and Kilbey, 1995; Foley et al., 2001). Similar complexities are evident at Ridgeway, which contains gold in pyrite disseminated primarily in cherts, gold in pyrite-bearing and silicified layers in tuffs, as well as gold associated with hydrothermal and volcanic breccias (Gillon et. al., 1995, 1998). Lacking such complications is the Barite Hill deposit, which is widely accepted as an example of a gold-rich volcanogenic massive sulfide deposit (Clark et al., 1999).

Brewer

The Brewer deposit is the best example of high-sulfidation epithermal-style gold mineralization in the slate belt (Fig. 2). Gold-pyrite-chalcopyrite-enargite ores in breccias are associated with subvolcanic quartz porphyry that intruded

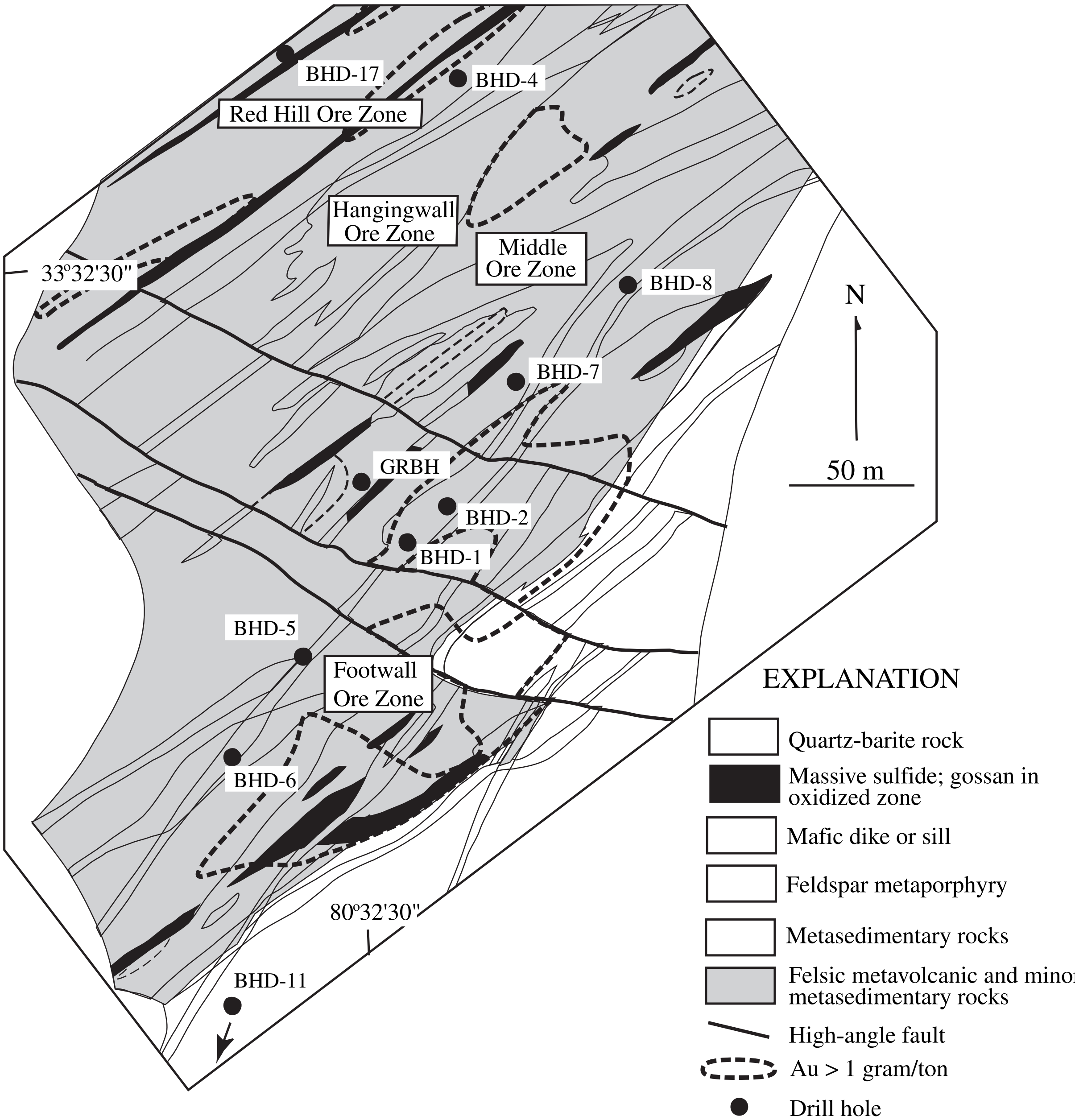

FIG. 5. Generalized geologic map of the Main pit area of the Barite Hill gold deposit (modified from Clark et al., 1999; and Seal et al., 2001).

rhyodacite to rhyolitic flows and tuffs equivalent to the Persimmon Fork Formation (Scheetz, 1991; Zwaschka and Scheetz, 1995). Leaching produced advanced argillic, sericitic, and propylitic hydrothermal alteration zones. The Brewer pit contains mostly andalusite-quartz rock and sulfide-bearing breccia (Fig. 2). Pyrophyllite, andalusite, and kyanite, together with kaolinite and sericite are commonly found in association with plutonic rocks in the region, but their exact relationship to mineralizing events is unclear. At Brewer, andalusite could have formed from reactions of felsic wall rock and hydrothermal fluids or during burial (Scheetz, 1991). Gold mineralization is related to the quartz porphyry breccias (Fig. 6A) and particularly with the medium- to coarse-textured heterolithic volcanic crystal tuff breccias in the argillic alteration zone (quartz-andalusite-pyrite-alunite-dickite-topaz-rutile; Fig. 2). The fine- to medium-textured breccia is associated with irregular and discontinuous lenses of massive quartz topaz breccia that locally contain abundant fine-grained zircon and rutile (Zwaschka and Scheetz, 1995). A high-temperature assemblage consisting of chalcopyrite-pyrite-bismuthinite is coeval with pyrite-enargite-covellite-electrum (Fig. 6B). A later, lower temperature assemblage consists of electrum-iron oxides-alunite ± jarosite. Galena occurs with pyrite and enargite and with chlorite and calcite in veins. The B6 pit contains massive sulfide-gossan (primary host of the gold) and andalusite-quartz breccia.

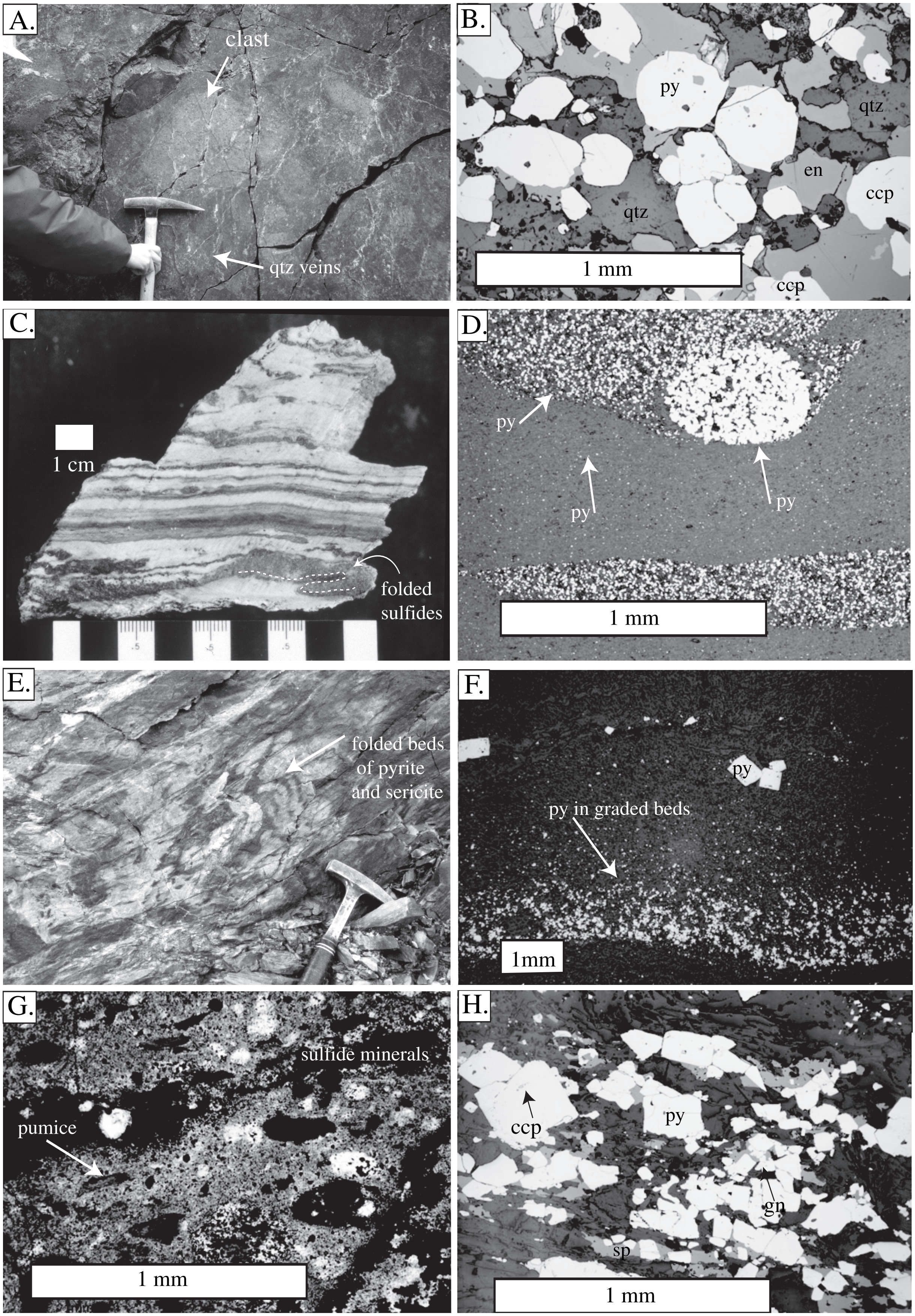
A.
clast
qtz veins
B.
py
qtz
en
ccp
qtz
1 mm
ccp
C.
1 cm
folded sulfides
D.
py
py
py
1 mm
E.
folded beds of pyrite and sericite
F.
py
py in graded beds
1mm
G.
sulfide minerals
pumice
1 mm
H.
ccp
py
gn
sp
1 mm

Haile

Gold was mined from siliceous pods and semimassive sulfide bodies metamorphosed to middle greenschist facies within various deposits (Speer and Maddry, 1993; Maddry and Kilbey; 1995; Fig. 3). The primary gold host is the Haile metasiltstone unit (laminated metamudstone enclosing bodies of fine-grained to cryptocrystalline silica). This unit is interlayered with rhyolitic crystal tuffs, undifferentiated volcaniclastic rocks (crystal and lithic tuffs), and volcaniclastic arenite of the Persimmon Fork Formation. The overlying Richtex Formation does not contain gold mineralization or hydrothermal alteration. The Champion pit differs from most other deposits because the gold mineralization is hosted by quartzose arenites (and metavolcanic rocks?), and because it is thought to be associated with a subvolcanic breccia pipe (high-grade gold core) interpreted as a hydrothermal vent (Speer and Maddry, 1993).

The highest gold contents are associated with pyrite oriented along cleavage in deformed rocks and with medium- to coarse-grained pyrite mixed with silica. Also recognized are undeformed sedimentary beds with fine-grained pyrite, syngenetic massive to semimassive bodies with very fine grained pyrite adjacent to or below gold ore, and disseminated coarse-grained pyrite cubes (Speer and Maddry, 1993; Worthington, 1993; Foley et al., 2001). Pyrite in folded laminae (oldest generation of sulfides) predates Paleozoic deformation (e.g., Offield, 1994; Fig. 6C). Folding of finely laminated, graded beds of pyrite-sericite-quartz has been cited as evidence of synvolcanic pyrite and contemporaneous sericitic alteration (Foley et al., 2001) and against a replacement origin (Tomkinson, 1988; Hayward, 1992). Pyrite replaced flattened pumice that contains chalcopyrite and pyrrhotite. Significantly, some pyrite contains blebs of electrum (<5 μm) and retains zoning in arsenic (Foley et al., 2001). The gold-bearing pyrite was affected by regional metamorphism that remobilized sulfides (Fig. 6D) and further concentrated gold in structurally favorable sites (Speer and Maddry, 1993). Gold in quartz and pyrite-rich rocks occurs with accessory molybdenite, rutile, and K-feldspar. Fe sulfide minerals, electrum, and molybdenite are syngenetic. Additional Fe sulfide minerals, gold, chalcopyrite, arsenopyrite, and Au and Ag tellurides formed later. Galena occurs primarily as inclusions in pyrite in the predeformation stages. Hydrothermal K-feldspar (Hardy, 1989) occurs in quartz veins with the early sulfide assemblages.

Ridgeway

Gillon et al. (1998, and references therein) have shown that the gold deposits are found in a basin containing the transition from pyroclastic felsic volcanism (Persimmon Fork Formation) to submarine and predominantly mafic volcanism and turbidite sedimentation (Richtex Formation). The North pit includes metasedimentary and felsic metavolcanic rocks. The South pit contains predominantly metasedimentary rocks with minor felsic metavolcanic rocks. In the North pit, gold concentrations are highest in the central potassic and silicic alteration zones that developed in thinly bedded turbidites. The dominant gold host is bluish-gray chert, containing fine-grained disseminated pyrite (and molybdenite?), and generally associated with minor felsic and mafic tuffs and volcanic and hydrothermal breccias. Eager et al. (1997) summarized evidence indicating that the gold mineralization is syngenetic (Fig. 4). The first generation of folding deformed hydrothermal, pyrite-bearing, and silicified layers (Fig. 6E). Pyrite also occurs as metacrysts enclosing fine-grained sulfides and silicates and in graded beds (Fig. 6F). Galena occurs as inclusions in pyrite and in quartz veins. An early generation of fine-grained (<5 μm) molybdenite is interleaved with pyrite-sericite laminae, but molybdenite also cuts replacement zones (Gillon et al., 1998). Coarse-grained molybdenite occurs with arsenopyrite in or along the margins of quartz veins and is also abundant where the ore-host phyllite is intensely deformed and veined.

Barite Hill

Stratiform gold-rich base metal (Fe, Zn, Cu, Pb)-barite mineralization at Barite Hill (Fig. 5) is hosted by intermediate to felsic metavolcanic rocks (crystal tuffs) and quartz feldspar porphyry (Lincolnton metadacite), which are overlain by metasedimentary and minor mafic metavolcanic rocks (Clark et al., 1999). The metavolcanic rocks (Fig. 6G) are equivalent to the Persimmon Fork Formation and the metasedimentary rocks to the Richtex Formation. Hypogene mineralization consists of lenses of massive barite (and quartz) or massive sulfide minerals (pyrite with minor chalcopyrite, sphalerite, galena (Fig. 6H), and bornite, and tennantite), and veinlets containing Au-Ag tellurides (including native gold, electrum, sylvanite, and other Au-Ag tellurides and base metal sulfides (galena and Cu-Fe sulfide minerals; Clark et al., 1999; Seal et al., 2001). Remnants of botryoidal pyrites and zoned colloform sphalerite occur within the

FIG. 6. A. Quartz porphyry breccia in the Brewer pit closely associated with gold and copper mineralization. Note large light-colored clasts of quartz porphyry in center of picture, which are cut by multiple generations of quartz veins. B. Thin section photograph showing rounded bright gray pyrite grains (py) enclosed by medium gray enargite (en), light gray chalcopyrite (ccp), and dark gray quartz (qtz; Brewer deposit). C. Rock sample showing alternating laminae of sericite (light gray) and pyrite (dark gray) from the Haile deposit. Folded fold crests and interference between fold pieces indicate two generations of isoclinal folding. D. Thin section photograph showing some of the multiple generations of pyrite commonly found in mineralized samples (Haile deposit). Coarse pyrite occurs in remobilized layers separated by pyrite-bearing mudstone. Layers contain pyrite pebbles. E. Felsic ash-flow tuff from the Persimmon Fork Formation in the North pit of the Ridgeway deposit, showing silicification of layers (light gray) marking isoclinal folds with well-developed axial-plane cleavage. Small isoclinal folds wrap the crest of the large folds. Silicification associated with the gold mineralizing event predated the first generation of folds (Offield, 1994). F. Thin section photograph showing layering typical of mineralized zones (Ridgeway deposit). Note sedimentary layering and graded bedding in fine pyrite crystals (bright gray). G. Thin section photograph showing remnants of volcanic textures (pumice fragments, light gray) and sulfide minerals (black; Barite Hill deposit). H. Thin section photograph showing large angular crystals of pyrite (py) containing blebs and stringers of sphalerite (sp), chalcopyrite (ccp), and galena (gn; Barite Hill deposit).

massive sulfide and barite zones (Foley et al., 2001, and unpub. data). In the Main pit, massive sulfide and quartz-barite lenses are distributed in four ore zones: Footwall, Middle, Hangingwall, and Red Hill (Fig. 5). Rocks containing abundant barite, pyrite, galena, and sphalerite have the highest gold contents, an association that is similar to that of other submarine, volcanogenic gold-rich massive sulfides. Gold production predominantly comes from the oxidized ore zones (quartz, hematite, goethite, and late-stage barite).

Previous Work

Igneous and sedimentary rocks in the vicinity of the Neoproterozoic gold deposits of the Carolina slate belt have been the focus of geochronologic studies since at least the 1980s (e.g., Fullagar, 1981; Fullagar et al., 1987; McSween et al., 1991). The Persimmon Fork Formation in central South Carolina is thought to be ca. 550 Ma (e.g., Dennis, 1995). Near the Ridgeway deposit (~20 km southwest), a quartz-feldspar crystal-lapilli metatuff has a zircon U-Pb age of 550.5 ± 5.9 Ma (Barker et al., 1998), and near the Barite Hill deposit, a hypabyssal intrusion (Lincolnton metadacite) emplaced into cogenetic volcanic rocks of the Persimmon Fork Formation has a zircon U-Pb age of 566 ± 15 Ma (Carpenter et al., 1982).

Ar-Ar geochronology and common Pb results (Ayuso et al., 1999) from the Brewer, Haile, and Ridgeway gold deposits are consistent with Paleozoic heating and isotopic disturbance (e.g., Horton et al., 1989), although they cannot be used to establish the ages of crystallization of the volcanic rocks or the gold mineralization. These estimates, as well as those using the whole-rock Rb-Sr (e.g., Butler and Secor, 1991, and references therein) and U-Th-Pb methods (LeHuray, 1987) are younger and less precise than zircon ages of volcanic rocks hosting the ore deposits reported here. Constraints on the age of mineralization are provided by Re-Os dating of molybdenite from the Haile deposit that yielded ages of 563 ± 2 and 596 ± 2 Ma (Maddry and Kilbey, 1995), amended to 553.8 ± 9 and 586.6 ± 3.6 Ma (Stein et al., 1997). Also, Re-Os molybdenite ages from the Ridgeway deposit include 551.9 ± 2.6 and 557.9 ± 3.3 Ma (Stein et al., 1997).

Sampling

Analyses of zircons were carried out using the SHRIMP-RG on five samples: two from the Brewer mine, two from Haile, and one from Ridgeway. Samples from Brewer include quartz-topaz rhyolite breccia (BR2B) from the argillic zone (Brewer pit) and felsic ash-flow tuff hosting gold mineralization (RA972; Fig. 2). Two samples of crystal lithic rhyolitic ash-flow tuffs interbedded with metasedimentary (quartz-arenite) layers from the Champion pit in the Haile deposit were obtained: RA975 and RA976 (Fig. 3). Both were collected from the same large outcrop. The sample from Ridgeway is a felsic ash-flow tuff (RIDN99) from the stratigraphic host of the North pit gold deposit (unit 6 of Gillon et al., 1998; Fig. 4).

Sulfide minerals (galena, pyrite, enargite, sphalerite, chalcopyrite, and molybdenite) and silicate minerals (K-feldspar and sericite) from all paragenetic stages were used for Pb isotope analysis. More than 250 new analyses were obtained. Pb isotope data were also collected for the Persimmon Fork Formation.

Analytical Procedures

Application of traditional U-Pb zircon dating proved difficult because of zircon yields and crystal imperfections. The zircons are corroded and frosted and contain open spherical pits (vacuoles?) with epitaxial molybdenite, pyrite, and sericite, among other minerals (Fig. 7). As a result of the crystal complexities, we employed ion microprobe techniques for optimum spatial resolution. First, a survey of zircons was carried out using the ion microprobe at the University of California, Los Angeles; subsequent detailed studies employed the Stanford-U.S. Geological Survey SHRIMP-RG (sensitive high mass-resolution ion microprobe-reverse geometry). Reviews of the applied techniques are in Williams (1996). The SHRIMP-RG differs from other SHRIMP instruments because of its reverse geometry design. An electrostatic mass analyzer downstream of the magnet permits third-order focusing, resulting in improved mass resolution (Williams, 1996; Bacon et al., 2000).

Rocks from surface outcrops (20 kg or more) were crushed and processed using standard mineral separation techniques. Single zircons and fragments were examined for imperfections (cracked and cloudy grains) and inclusions using cathodoluminescence techniques on a JEOL 840 scanning electron microprobe. Zircons were mounted in epoxy, polished, photographed, and coated with ~10 nm of gold. Polished mounts were cleaned with soap, 1*N* HCl, and distilled water and dried prior to coating with gold. A primary beam of $^{16}O_2^-$ ions (about 10–20 nA) was used to raster an area about 50 × 50 μm for about 90 s to remove the gold coat and surface contamination (common Pb). Results show that ^{204}Pb is typically <0.01 percent of total Pb. The beam was focused to create flat-floored (about 2-μm-deep) elliptical pits for analysis (about 30 × 35 μm). The intensity of the $^{238}U^{16}O$ peak was monitored to select appropriate zircon grains that had been chosen using a scanning electron microscope. A very small amount of sample was obtained (less than 2 ng) as positive secondary ions and measured by the mass spectrometer. Data were collected for five to seven scans per spot for $^{90}Zr_2{}^{16}O$, ^{204}Pb, ^{206}Pb, ^{207}Pb, ^{238}U, $^{232}Th^{16}O$, and $^{238}U^{16}O$ for 2 to 20 s for each peak. Results for each oxide were formulated to an atomic basis using the relationship of $^{232}Th/^{238}U = 1.11 \times ThO^+/UO^+$ (Ireland, 1994). Data from each spot were referenced to the 1,099 Ma zircon standard AS57 from the Duluth gabbro (Paces and Miller, 1993). Replicate analyses of zircon standard SL13 from Sri Lanka were used to calibrate U and Th, resulting in an estimated elemental abundance accuracy of ~20 percent in our samples; AS57 was used for age calibrations. Common Pb used for age correction is from Cumming and Richards (1975). Zircon and Pb isotope data were reduced using the programs PRAWN and LEAD (Ireland, 1994) and ISOPLOT/EX (Ludwig, 1999). Analytical results of the geochronology study are presented in Tables 1, 2, and 3.

About 10 to 50 mg of each mineral was dissolved in HNO_3-HCl or in HF. Pb isotopes were purified using standard procedures (Ayuso et al., 2003) and were measured in static mode with a multicollector, automated Finningan MAT-262 mass spectrometer at the U.S. Geological Survey, Reston, VA. Pb isotope ratios were corrected for mass fractionation by

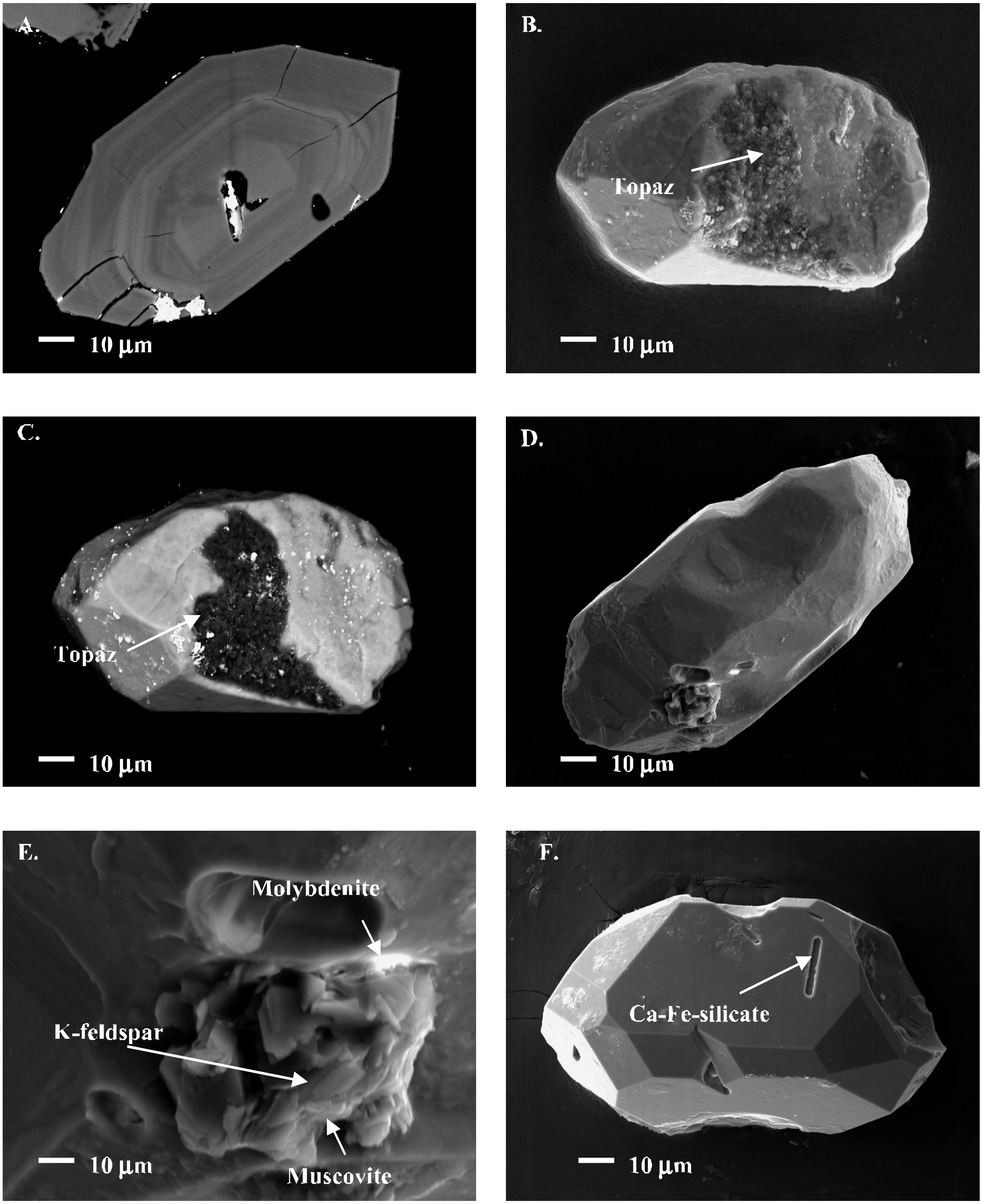

FIG. 7. Backscattered electron (BSE) and secondary electron (SE) images of zircons. A. Brewer: BSE image of subhedral zircon (sample BR2B) with subtle zoning in mean atomic mass, microcracks, and inclusions in outer rim. B. Brewer: Subrounded zircon (sample BR2B) encrusted with hydrothermal minerals. C. SEM-BSE image of (B) shows that the crust is dominantly composed of hydrothermal topaz (dark phase), which is distributed across the zircon surface. D. Haile: BSE image of subhedral zircons (sample RA976) containing empty pits in core and subtle zoning. E. SE image closeup (rotated) of pit in (D) containing platy muscovite, blebs of molybdenite, and blocky K-feldspar. F. Ridgeway: SE image of zircon (sample RIDN99) showing zoning, microcracks, and large solid inclusion of Ca-Fe silicate.

TABLE 1. U-Pb Isotope Data for Zircons from Samples BR2B and RA97-2, Brewer Deposit, South Carolina

Grain.spot	U[1] (ppm)	Th (ppm)	Th/U	^{204}Pb (ppb)	^{207}Pb/^{206}Pb	Error[2]	^{238}U/^{206}Pb	Error[2]	Age (Ma)	Error[3]
BR2B-1.1	185	130	0.70	26	0.0797	0.0013	11.65	0.15	517.1	6.5
BR2B-3.1i	391	368	0.94	12	0.0635	0.0007	11.18	0.14	548.9	6.7
BR2B-4.1i	213	154	0.72	13	0.0679	0.0012	11.05	0.15	552.5	7.0
BR2B-5.1	523	583	1.12	26	0.0659	0.0008	12.67	0.27	484.5	10.1
BR2B-6.1	146	80	0.55	14	0.0771	0.0013	10.52	0.18	572.9	9.2
BR2B-7.1i	123	74	0.61	21	0.1000	0.0014	10.51	0.16	557.2	8.2
BR2B-9.1i	179	129	0.72	15	0.0732	0.0015	11.05	0.16	549.0	7.5
BR2B-10.1	212	204	0.96	27	0.0808	0.0011	11.46	0.18	524.7	7.8
BR2B-11.1	155	128	0.83	38	0.0896	0.0018	14.05	0.28	425.2	8.1
BR2B-12.1i	69	42	0.60	19	0.1045	0.0035	10.63	0.20	548.3	10.0
BR2B-14.1i	220	128	0.58	23	0.0784	0.0019	10.92	0.15	551.5	7.3
BR2B-15.1i	169	96	0.57	20	0.0754	0.0010	11.03	0.16	548.5	7.7
BR2B-16.1	359	297	0.83	9	0.0652	0.0007	10.94	0.13	559.7	6.4
BR2B-16.2	303	256	0.85	34	0.0731	0.0011	11.21	0.15	541.3	6.9
BR2B-17.1i	318	343	1.08	18	0.0697	0.0007	10.93	0.13	557.1	6.6
BR2B-18.1	122	90	0.74	23	0.0954	0.0027	13.21	0.31	448.3	10.2
BR2B-19.1	441	430	0.98	73	0.0861	0.0013	11.87	0.13	503.6	5.5
BR2B-20.1	428	503	1.18	148	0.1190	0.0010	10.18	0.12	561.6	6.6
BR2B-21.1	399	306	0.77	68	0.0841	0.0010	16.21	0.21	371.9	4.7
BR2B-21.2	128	105	0.82	11	0.0767	0.0011	11.40	0.20	530.2	9.0
BR2B-23i	131	94	0.72	7	0.0702	0.0009	11.24	0.20	541.9	9.5
BR2B-24.1/1.1i	357	457	1.28	12	0.0659	0.0008	11.33	0.15	545.2	7.0
BR2B-25.1	449	602	1.34	7	0.0662	0.0010	11.47	0.19	539.1	8.6
BR2B-26.1	195	187	0.96	5	0.0629	0.0011	11.69	0.20	529.1	8.8
BR2B-27.1i	207	143	0.69	0	0.0602	0.0010	11.26	0.16	548.5	7.5
BR2B-30.1i	172	135	0.78	7	0.0633	0.0013	11.11	0.20	555.6	9.6
BR2B-31.1	663	781	1.18	124	0.0730	0.0009	17.59	0.20	356.5	3.9
BR2B-32.1i	179	91	0.51	0	0.0592	0.0011	11.02	0.20	559.9	9.8
BR2B-33.1	554	713	1.29	9	0.0600	0.0006	11.09	0.08	556.5	3.9
BR2B-36.1	153	162	1.06	56	0.1503	0.0038	12.42	0.24	499.3	9.4
BR2B-37.1	641	713	1.11	9	0.0614	0.0011	10.86	0.08	568.0	4.0
BR2B-39.1i	595	599	1.01	26	0.0645	0.0009	11.25	0.09	549.2	4.4
BR2B-40.1	467	541	1.16	6	0.0595	0.0013	11.64	0.15	531.3	6.7
BR2B-41.1	639	821	1.29	90	0.0680	0.0015	13.05	0.24	476.0	8.4
BR2B-43.1i	541	621	1.15	0	0.0593	0.0008	11.35	0.16	544.4	7.3
BR2B-44.1	242	176	0.73	13	0.0672	0.0017	11.73	0.19	527.5	8.2
BR2B-45.1	358	422	1.18	20	0.0712	0.0011	11.77	0.14	525.6	6.0
BR2B-46.1	262	221	0.84	20	0.0747	0.0012	11.74	0.20	527.1	8.7

Weighted mean age for BR2B at 2σ (n = 15, MSWD = 1.6) = 550.2 ± 2.5 Ma

about 0.12 percent amu^{-1} according to replicate measurements of NBS 981 (n = 27). Total precision (2σ) is estimated to be better than about 0.012 for ^{206}Pb/^{204}Pb, 0.017 for ^{207}Pb/^{204}Pb, and 0.050 for ^{208}Pb/^{204}Pb. Total Pb blanks during the course of this study were less than 50 pg and thus are insignificant relative to the Pb abundances in the sulfide and silicate minerals. Pb isotope data are listed in the Appendix.

Results

Zircon petrography

Topaz rhyolite at the Brewer pit (Fig. 2) contains clear, fine-grained (60–160 μm), pink to yellow equant zircons. Acicular and fine-grained zircons (10–20 μm) also occur. Zircons display euhedral growth zoning or complex sector zoning and lack rounded cores or inclusions indicating inherited domains (Fig. 7A). Backscattered electron imaging illustrates fine scale to broad zoning that correlates with substitution of Hf. About 70 zircons were obtained from topaz rhyolite sample BR2B. Sample RA972 produced about 70 zircon grains (most <165 μm). Microcracks in these zircons are common (Fig. 7A). Cavities and pits (vacuoles?) etched on the zircon surface contain very fine grained quartz, sericite, pyrite, cassiterite, topaz, K-feldspar, and other unknown phases (Fig. 7B). Topaz also occurs as crusts on corroded and frosted zircons (Fig. 7C). These surface defects suggest considerable reaction between zircons and hydrothermal solutions during alteration and mineralization or Paleozoic metamorphic disturbances.

Zircons from crystal lithic rhyolitic ash-flow tuffs from the Champion pit of the Haile deposit (Fig. 7D) are stubby to elongate (~120 μm), light yellow and pink, and contain inclusions. Some zircons have pits containing platy muscovite, molybdenite, and K-feldspar (Fig. 7E). Zircons from a felsic ash-flow tuff from the North pit at Ridgeway are subhedral, stubby to elongate, colorless to pale pink and light brown (Fig. 7F). Sample RIDN99 yielded about 60 zircons (most <150 μm). Cavities and pits contain sericite (?) and K-feldspar.

Zircon analyses

As a result of the overall fine-grain size of the zircons and the occurrence of fractures, crystal imperfections, corrosion, inclusions, cavities, and pits, only one spot (~25–30 μm) was analyzed from most zircons. Even at this scale, it was difficult to avoid inclusions and irregularities (probably accounting for

TABLE 1. (*Cont.*)

Grain.spot	U[1] (ppm)	Th (ppm)	Th/U	^{204}Pb (ppb)	^{207}Pb/^{206}Pb	Error[2]	^{238}U/^{206}Pb	Error[2]	Age (Ma)	Error[3]
RA97-2-1.1	159	211	1.33	17	0.0889	0.0018	19.26	0.38	312.0	6.1
RA97-2-2.1i	135	74	0.55	14	0.0819	0.0017	10.78	0.20	556.4	9.8
RA97-2-2.2	183	134	0.74	6	0.0641	0.0012	10.79	0.20	568.0	9.9
RA97-2-4.1	162	98	0.60	9	0.0683	0.0011	10.60	0.17	574.9	8.9
RA97-2-6.1i	132	132	1.00	12	0.0743	0.0014	11.04	0.21	548.5	9.8
RA97-2-7.1i	67	42	0.62	8	0.0850	0.0022	10.97	0.17	545.0	8.2
RA97-2-7.2	46	31	0.67	8	0.0934	0.0029	10.38	0.20	568.9	10.5
RA97-2-8.1i	299	208	0.70	12	0.0651	0.0012	11.29	0.15	542.8	7.0
RA97-2-9.1i	114	71	0.62	17	0.0882	0.0018	10.90	0.20	545.9	9.5
RA97-2-10.1i	162	177	1.09	48	0.1158	0.0016	10.44	0.14	550.1	7.2
RA97-2-10.2i	157	164	1.04	11	0.0717	0.0014	10.96	0.14	554.5	6.8
RA97-2-12.1	79	62	0.78	34	0.1252	0.0089	9.89	0.20	572.7	13.0
RA97-2-13.1i	97	48	0.50	11	0.0807	0.0016	11.01	0.18	545.9	8.6
RA97-2-15.1i	102	69	0.68	11	0.0783	0.0011	10.89	0.17	553.3	8.5
RA97-2-17.1i	302	344	1.14	14	0.0672	0.0011	11.11	0.15	549.8	7.0
RA97-2-18.1	379	194	0.51	20	0.0684	0.0016	15.21	0.24	403.9	6.2
RA97-2-19.1	254	136	0.54	6	0.0636	0.0008	10.71	0.18	572.6	9.4
RA972-20.1i	351	228	0.65	3	0.0596	0.0008	11.10	0.12	553.9	5.7
RA972-21.1	292	578	1.98	1	0.0551	0.0019	20.89	0.39	299.5	5.5
RA972-22.1	222	195	0.88	7	0.0599	0.0013	11.69	0.18	526.4	7.8
RA972-23.1	704	135	0.19	4	0.0788	0.0010	5.10	0.04	1147.9	8.4
RA972-24.1	440	549	1.25	1	0.0582	0.0007	11.66	0.23	528.8	10.1
RA972-25.1	281	195	0.69	0	0.0574	0.0009	11.93	0.19	517.3	7.9
RA972-27.1	353	481	1.36	0	0.0591	0.0020	12.17	0.18	506.4	7.2
RA972-29.1	425	393	0.93	5	0.0599	0.0011	11.84	0.13	519.9	5.4
RA972-30.1	384	587	1.53	1	0.0594	0.0013	11.74	0.20	524.3	8.5
RA972-31.1	66	68	1.04	0	0.0735	0.0022	12.73	0.28	476.1	10.0

Weighted mean age for RA972 at 2σ (n = 11, MSWD = 1.3) = 550 ± 3 Ma

Notes: MSWD = mean square of weighted deviates; i = sample included in preferred weighted mean age calculation; U-Pb constants by Steiger and Jäeger (1977)

[1]Concentrations of U and Th analyzed using the SHRIMP-RG

[2]Absolute counting errors (1σ)

[3]Error in millions of years

the somewhat higher ^{204}Pb contents in some analyses). A total of 38 zircons were analyzed from sample BR2B and 27 from sample RA972 from Brewer (Table 1). Zircons from sample BR2B show scattered ^{206}Pb/^{238}U ages from about 340 to 580 Ma, with a major group of 26 analyses at about 520 to 560 Ma (Table 1). Nine zircon analyses younger than about 520 Ma and two older than 575 Ma could be excluded from the age calculation if they reflect Pb loss or new growth (possibly accounting for the younger ages) and if they include a small amount of inheritance (thus accounting for the older ages). Petrographic examination did not reveal anything that would warrant discarding these results. However, analytical outliers were identified and discarded if the results exceeded 4σ from the mean or deviated from a normal distribution on a probability plot. Selection of analyses in this manner results in a weighted average ^{206}Pb/^{238}U age of 546 ± 5 Ma (mean square of the weighted deviates, MSWD = 10.7; n = 27). Restricting the results used for the age calculation to consist only of analyses from the major group of 26 samples and to analyses that agree to within each of their analytical errors gives a weighted mean ^{206}Pb/^{238}U age of 550 ± 3 Ma (95% confidence; MSWD = 1.6, n = 15; Fig. 8A).

For sample RA972, the ^{206}Pb/^{238}U ages range from about 300 to 575 Ma, with a large group from about 500 to 575 Ma and one analysis yielding an age of 1148 Ma (Table 1). Eliminating outliers in the same manner as above results in a weighted average ^{206}Pb/^{238}U age of 549 ± 6 (MSWD = 9.7; n = 18). Analyses from the dominant group and those that are consistent to within each of their analytical errors produced a weighted mean age of 550 ± 3 Ma (MSWD = 1.3, n = 11; Fig. 8C). Although the ^{207}Pb/^{206}Pb ages of these zircons are not precise enough for comparison to the ^{206}Pb/^{238}U ages (e.g., Sambridge and Compston, 1994), an age estimate can be obtained from Tera-Wasserburg plots (Fig. 8B, D; Tera and Wasserburg, 1972). The dominant group of ^{206}Pb/^{238}U ages for samples BR2B and RA972 has concordia intercepts at 547 ± 5 Ma (MSWD = 2.0, n = 15), and 549 ± 6 Ma (MSWD = 1.6, n = 11), analytically indistinguishable from the weighted mean ^{206}Pb/^{238}U ages of about 550 ± 3 Ma. This is interpreted as the age of crystallization of the topaz rhyolite and a close estimate of the age of mineralization in the Brewer deposit.

A total of 37 zircons were analyzed from sample RA975 and 30 from sample RA976 from the Champion pit of the Haile deposit (Table 2). Samples RA975 and RA976 also show scattered ^{206}Pb/^{238}U ages from about 358 to 658 Ma, with a predominant group at about 481 to 577 Ma and one analysis at about 1832 Ma. Excluding zircon analyses in both samples using the same approach as above results in a weighted mean ^{206}Pb/^{238}U age of 549 ± 4 Ma (MSWD = 9; n = 44). Spot analyses forming the major group and those that agree to within experimental errors for sample RA975 result in a weighted mean ^{206}Pb/^{238}U age of 552 ± 4 Ma (MSWD = 2.5,

TABLE 2. U-Pb Isotope Data for Zircons from Samples RA975 and RA976, Haile Deposit, South Carolina

Grain.spot	U[1] (ppm)	Th (ppm)	Th/U	^{204}Pb (ppb)	^{207}Pb/^{206}Pb	Error[2]	^{238}U/^{206}Pb	Error[2]	Age (Ma)	Error[3]
RA975-1.1	85	49	0.57	7	0.0730	0.0011	10.66	0.15	568.7	7.9
RA975-2.1	120	94	0.78	4	0.0648	0.0018	10.72	0.21	571.1	10.9
RA975-3.1	126	80	0.63	8	0.0717	0.0010	9.20	0.14	657.5	9.6
RA975-4.1i	110	92	0.83	16	0.0851	0.0023	10.81	0.19	552.8	9.5
RA975-4.1i	253	186	0.74	1	0.0602	0.0009	11.19	0.14	551.2	6.5
RA975-5.1i	174	163	0.94	6	0.0656	0.0014	10.95	0.17	558.9	8.3
RA975-5.1a	209	283	1.36	0	0.0587	0.0011	11.65	0.18	531.4	7.8
RA975-7.1	155	112	0.73	12	0.0737	0.0014	12.04	0.25	504.5	10.3
RA975-7.1	244	172	0.70	338	0.1279	0.0010	2.79	0.05	1831.6	26.8
RA975-9.1i	116	71	0.61	4	0.0656	0.0014	10.99	0.24	556.7	11.8
RA975-9.1a	203	168	0.83	12	0.0728	0.0014	13.54	0.17	451.9	5.7
RA975-11.1	132	109	0.83	38	0.1230	0.0031	13.74	0.24	416.2	7.2
RA975-11.1a	182	120	0.66	0	0.0594	0.0011	9.98	0.21	615.3	12.1
RA975-12.1	500	612	1.22	3	0.0602	0.0010	10.95	0.10	562.6	5.1
RA975-13.1	172	141	0.82	2	0.0616	0.0020	11.48	0.21	536.9	9.6
RA975-14.1	244	251	1.03	0	0.0594	0.0011	11.42	0.19	541.0	8.6
RA97-14.1i	442	467	1.06	57	0.0819	0.0012	10.73	0.18	558.7	8.9
RA97-15.1	208	230	1.11	8	0.0657	0.0013	11.52	0.22	531.9	9.9
RA97-16.1i	358	330	0.92	9	0.0636	0.0007	11.09	0.15	553.4	7.2
RA975-16.1	186	280	1.51	4	0.0629	0.0029	10.64	0.44	576.9	7.7
RA975-17.1i	188	167	0.89	2	0.0611	0.0011	11.19	0.16	550.8	7.8
RA975-18.1i	129	92	0.71	2	0.0624	0.0015	11.20	0.21	549.2	10.0
RA975-18.1i	111	100	0.90	14	0.0816	0.0019	10.80	0.27	555.5	13.2
RA975-19.1i	333	199	0.60	14	0.0667	0.0008	11.19	0.20	546.5	9.1
RA975-19.1a	212	332	1.57	14	0.0701	0.0009	9.96	0.16	609.7	9.2
RA975-19.1bi	308	380	1.24	15	0.0690	0.0029	11.08	0.14	550.5	7.1
RA975-20.1	194	154	0.80	4	0.0624	0.0016	10.72	0.19	572.8	10.0
RA975-21.1	192	147	0.76	0	0.0590	0.0015	10.85	0.13	568.8	6.4
RA975-21.1i	138	96	0.69	5	0.0654	0.0016	10.97	0.21	557.9	10.1
RA975-22.1i	132	85	0.64	10	0.0731	0.0014	10.85	0.24	558.6	11.9
RA975-23.1i	152	121	0.80	22	0.0848	0.0018	10.76	0.21	555.4	10.3
RA975-23.1	536	1090	2.04	4	0.0606	0.0011	9.95	0.16	616.4	9.6
RA975-24.1	322	385	1.20	3	0.0613	0.0012	11.81	0.16	522.8	6.8
RA975-24.1	144	138	0.96	21	0.0846	0.0028	10.62	0.18	562.8	9.5
RA975-25.1i	159	139	0.88	3	0.0626	0.0015	11.06	0.20	555.4	9.8
RA975-25.1	637	1017	1.60	77	0.0852	0.0015	12.00	0.10	500.2	4.2
RA975-6.1	138	133	0.96	1	0.0608	0.0014	11.56	0.23	533.9	10.3

Weighted mean age for RA975 at 2σ (n = 15, MSWD = 0.72) = 553.5 ± 2.3 Ma

n = 19). For sample RA976 the weighted mean ^{206}Pb/^{238}U age is 549 ± 4 Ma (MSWD = 3, n = 9; Table 2). Combining the results for samples RA975 and RA976 results in a weighted mean ^{206}Pb/^{238}U age of 553 ± 2 Ma (MSWD = 0.95, n = 20; Fig. 8E). Combined ^{206}Pb/^{238}U ages for samples RA975 and RA976 have Tera-Wasserburg concordia intercepts at 551 ± 3 Ma (MSWD = 0.87, n = 20; Fig. 8F). This age is close to the weighted mean ^{206}Pb/^{238}U age of about 553 ± 2 Ma, which is interpreted as the age of crystallization of the volcanic rocks and a close estimate of the age of mineralization of the Champion pit in the Haile deposit.

Forty-seven zircon analyses were obtained from sample RIDN99 from Ridgeway (Table 3). Scattered ^{206}Pb/^{238}U ages range from about 350 to 754 Ma, with most analyses at about 520 to 580 Ma and one sample at about 1427 Ma. Outliers can be eliminated as illustrated above, resulting in a weighted average ^{206}Pb/^{238}U age of 553 ± 3 Ma (MSWD = 5.6, n = 35). Spot analyses from the major group that agree to within each of their analytical errors result in a weighted mean ^{206}Pb/^{238}U age of 556 ± 2 Ma (MSWD = 1.1, n = 20; Fig. 8G). The weighted mean ^{206}Pb/^{238}U age of 556 ± 2 Ma is interpreted as the age of crystallization of the volcanic rock and an estimate of the age of mineralization in the North pit of the Ridgeway deposit.

Pb isotopes

Pb isotope compositions of acid-leach aliquots and residues of sulfide minerals and silicates representing all major paragenetic stages are summarized in the Appendix and Figure 9. The majority of the analyses (n ~250) were obtained on pyrite; galena is relatively rare. As a group, sulfides and silicates straddle the average crustal Pb evolution curve (μ = ^{238}U/^{204}Pb = 9.74; Stacey and Kramers, 1975). Galena and K-feldspar plot near the least radiogenic end of their respective fields (Fig. 9); pyrite-leach compositions plot, for the most part, near the most radiogenic end of the pyrite field. Galena has a limited range in compositions and generally plots below the average crustal evolution curve, which generally represents the major reservoir of recycled continental crust. Calculated ^{238}U/^{204}Pb (μ) values for sulfides and silicates, relative to the two-stage model of Stacey and Kramers (1975), range mostly from 9.5 to 10; most model ages are younger than 540 Ma (some have future ages). Nearly all galenas have μ values lower than the

TABLE 2. *(Cont.)*

Grain.spot	U[1] (ppm)	Th (ppm)	Th/U	^{204}Pb (ppb)	^{207}Pb/^{206}Pb	Error[2]	^{238}U/^{206}Pb	Error[2]	Age (Ma)	Error[3]
RA976-1.1i	100	73	0.73	8	0.0738	0.0012	11.09	0.15	546.3	7.2
RA976-1.2	96	70	0.73	14	0.0847	0.0017	11.16	0.13	536.2	6.1
RA976-2.1	73	46	0.63	8	0.0786	0.0014	11.25	0.14	536.0	6.7
RA976-3.1	573	259	0.45	14	0.0615	0.0007	14.56	0.10	425.2	2.9
RA976-3.2	435	192	0.44	14	0.0634	0.0010	14.75	0.08	418.8	2.1
RA976-4.1i	109	66	0.61	13	0.0808	0.0014	11.13	0.21	539.8	9.6
RA976-7.1i	144	91	0.63	24	0.0888	0.0021	10.70	0.12	555.7	6.0
RA976-8.1	672	638	0.95	249	0.1504	0.0016	15.38	0.13	358.7	3.0
RA976-9.1	136	85	0.63	20	0.0865	0.0016	11.11	0.18	537.2	8.2
RA976-10.1	76	54	0.72	23	0.1101	0.0023	10.14	0.15	570.3	8.0
RA976-12.1i	103	81	0.78	16	0.0871	0.0015	10.86	0.10	548.9	5.1
RA976-13.1	191	122	0.64	201	0.2390	0.0040	10.02	0.12	480.5	6.2
RA976-14.1i	208	113	0.54	15	0.0719	0.0011	11.04	0.08	550.0	3.6
RA976-15.1	100	84	0.83	7	0.0710	0.0016	10.12	0.14	599.5	7.8
RA976-16.1i	162	58	0.36	31	0.0928	0.0019	10.94	0.18	540.8	8.4
RA976-17.1i	114	70	0.62	14	0.0808	0.0020	10.79	0.15	556.5	7.4
RA976-18.1	100	59	0.59	12	0.0795	0.0013	10.41	0.12	577.4	6.6
RA976-19.1	106	62	0.59	13	0.0812	0.0017	10.67	0.13	562.6	6.8
RA976-20.1	345	570	1.65	116	0.1429	0.0020	15.57	0.15	358.0	3.5
RA976-21.1	116	90	0.78	25	0.0975	0.0017	11.02	0.19	534.0	8.8
RA976-22.1	182	209	1.15	21	0.0773	0.0013	11.47	0.25	527.4	11.2
RA976-23.1i	316	353	1.12	10	0.0656	0.0012	11.09	0.19	552.5	9.0
RA976-24.1	277	183	0.66	76	0.1425	0.0033	15.43	0.31	364.7	7.3
RA976-25.1	153	107	0.70	0	0.0618	0.0019	12.42	0.27	497.6	10.4
RA976-28.1	123	101	0.82	2	0.0622	0.0018	12.09	0.31	510.5	12.5
RA976-29.1	355	203	0.57	3	0.0609	0.0011	11.60	0.16	531.8	7.2
RA976-30.1	402	296	0.74	66	0.0874	0.0012	11.15	0.09	535.5	4.3
RA976-31.1	1078	1235	1.15	264	0.0974	0.0008	11.94	0.09	495.3	3.8
RA976-31.1	190	214	1.13	2	0.0575	0.0011	10.92	0.17	566.2	8.3
	137	116	0.85	5	0.0595	0.0012	11.45	0.17	539.5	7.6

Weighted mean age for RA976 at 2σ (n = 8, MSWD = 2.5) = 548.9 ± 5.5 Ma

Notes: Weighted mean age at 2σ for samples RA975 and RA976 (n =20, MSWD = 0.95) = 552.6 ± 1.7 Ma MSWD = mean square of weighted deviates; i = sample included in preferred weighted mean age calculation, r = sample not included in weighted mean age calculation, U-Pb constants by Steiger and Jäeger (1977)

[1]Concentrations of U and Th analyzed using the SHRIMP-RG

[2]Absolute counting errors (1σ)

[3]Error in millions of years

average crustal Pb evolution curve (μ = 9.74) and attest to the mantle influence in the source of the Pb (deficient in ^{206}Pb and ^{207}Pb compared to much of the continental crust; Doe and Zartman, 1979). Values of μ higher than the average crustal curve point to a contribution from evolved isotopic reservoirs that are characteristic of the continental crust.

Pb isotope compositions of sulfides and silicates show extensive overlap and generally cannot be distinguished as a function of their paragenesis. For example, pyrite formed during the original mineralizing event in the Haile (e.g., Fig. 9C) and Ridgeway deposits (e.g., Fig. 9E) cannot be distinguished isotopically from remobilized pyrite (e.g., Fig. 9A). Enargite from Brewer is isotopically indistinguishable from coexisting pyrite (Fig. 9A-B). Molybdenite from Ridgeway can be among the least radiogenic minerals (Fig. 9E-F).

Discussion

Previous attempts to date the mineralization in the gold deposits from the slate belt by Ar-Ar, Pb-Pb, and Rb-Sr techniques yielded ages that are substantially younger than the zircon ages reported here. Re-Os molybdenite ages from Haile and Ridgeway (Maddry and Kilbey, 1995; Stein et al., 1997) in some cases closely approximate the U-Pb zircon ages of the volcanic rocks (553 ± 2 Ma for Haile and 556 ± 2 Ma for Ridgeway). Other Re-Os estimates can differ likely because of the complex paragenesis of molybdenite, as coatings and fillings along cleavage planes (Maddry and Kilbey, 1995; Gillon et al., 1998), in massive veins that cut across late fractures and faults, in association with pyrite in early pyrite-quartz and sericite-quartz laminae, and as inclusions in cavities in zircon grains.

Subsequent to the Neoproterozoic mineralizing events, pyrite and gold were remobilized into structural favorable sites as a result of folding. Reaction of the original sulfide minerals with fluids unrelated to the mineralizing event, transport and mobilization of the original common Pb in the sulfides, and mixing of radiogenic Pb, therefore, have obscured the initial isotopic compositions of the hydrothermal minerals (Fig. 10). However, sufficient Pb isotope information has survived to infer the source of the metals and to suggest possible modern tectonic analogues. Differences in ^{206}Pb/^{204}Pb among the sulfides within individual deposits could record in situ Pb growth since deposition, as a result of evolution under variable U/Pb and Th/Pb ratios. On a regional basis, isotopic differences among the deposits could also reflect the evolving composition of mineralizing fluids as

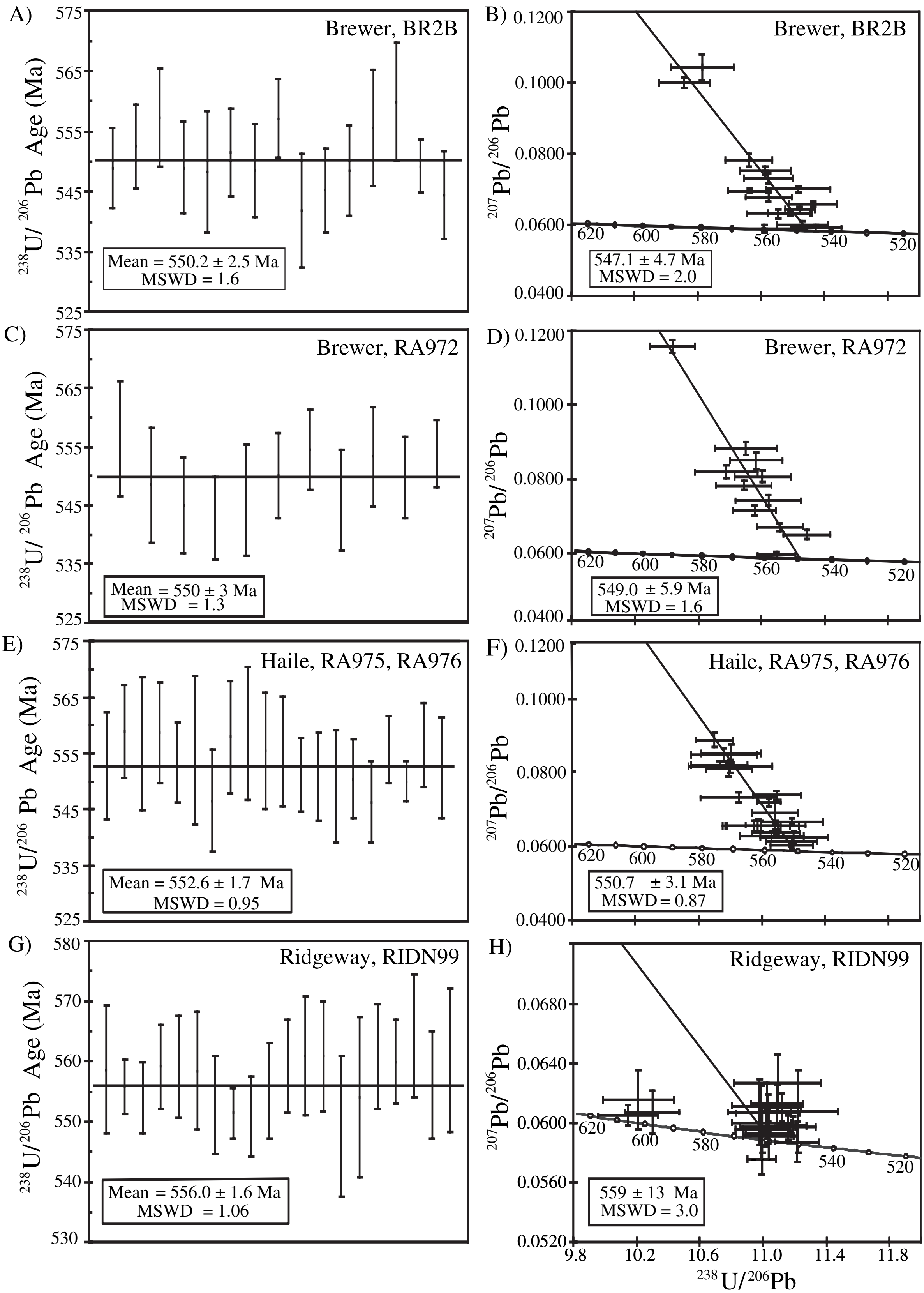

FIG. 8. Weighted average $^{206}Pb/^{238}U$ zircon ages and Tera-Wasserburg plots of U-Pb data. A. and B. Brewer sample BR2B (topaz rhyolite). C. and D. Brewer sample RA972 (ash-flow tuff). E. and F. Haile samples RA975 and RA976 (ash-flow tuff) from the Champion pit. G. and H. Ridgeway sample RIDN99 (ash-flow tuff).

TABLE 3. U-Pb Isotope Data for Zircons from Sample RIDN99, Ridgeway Deposit, South Carolina

Grain.spot	U[1] (ppm)	Th (ppm)	Th/U	^{204}Pb (ppb)	^{207}Pb/^{206}Pb	Error[2]	^{238}U/^{206}Pb	Error[2]	Age (Ma)	Error[3]
RIDN99-1.1	127	91	0.72	13	0.0800	0.0016	11.74	0.19	514.1	8.1
RIDN99-2.1	249	211	0.85	0	0.0587	0.0010	11.71	0.17	528.4	7.3
RIDN99-3.1	139	102	0.73	8	0.0705	0.0022	11.63	0.29	524.5	12.7
RIDN99-4.1	187	106	0.57	0	0.0586	0.0015	11.46	0.14	539.6	6.3
RIDN99-5.1	109	113	1.04	1	0.0617	0.0015	11.52	0.20	535.1	8.9
RIDN99-6.1i	117	88	0.75	1	0.0611	0.0015	11.02	0.22	558.6	10.6
RIDN99-7.1	275	164	0.60	1	0.0575	0.0008	10.72	0.13	576.2	6.6
RIDN99-8.1i	540	548	1.02	25	0.0575	0.0010	10.99	0.09	555.7	4.5
RIDN99-9.1i	368	616	1.67	2	0.0610	0.0010	11.12	0.12	554.0	5.9
RIDN99-10.1i	275	244	0.89	3	0.0593	0.0007	11.03	0.14	559.1	7.0
RIDN99-11.1i	151	135	0.90	1	0.0597	0.0012	11.03	0.17	559.1	8.5
RIDN99-12.1	159	142	0.89	0	0.0602	0.0013	10.83	0.20	568.5	9.9
RIDN99-13.1i	89	70	0.80	1	0.0606	0.0012	11.03	0.20	558.4	9.8
RIDN99-14.1i	238	247	1.04	0	0.0597	0.0008	11.16	0.17	552.8	8.2
RIDN99-15.1i	703	545	0.78	3	0.0598	0.0007	11.19	0.09	551.4	4.1
RIDN99-16.1	98	52	0.53	5	0.0590	0.0020	10.87	0.22	567.2	11.1
RIDN99-18.1	132	100	0.76	1	0.0644	0.0009	8.01	0.12	753.7	10.8
RIDN99-19.1i	350	246	0.70	0	0.0587	0.0013	11.22	0.14	550.9	6.6
RIDN99-20.1	570	822	1.44	41	0.0726	0.0011	11.04	0.08	550.0	3.8
RIDN99-21.1	287	332	1.16	3	0.0559	0.0009	14.69	0.20	426.1	5.7
RIDN99-22.1i	129	94	0.73	0	0.0613	0.0013	11.09	0.16	555.2	7.9
RIDN99-23.1i	193	188	0.97	2	0.0591	0.0016	11.04	0.16	559.2	7.8
RIDN99-24.1i	63	27	0.43	2	0.0607	0.0022	10.98	0.20	560.9	9.8
RIDN99-25.1i	127	87	0.69	2	0.0600	0.0025	10.99	0.19	560.8	9.2
RIDN99-26.1	476	376	0.79	0	0.0585	0.0012	11.81	0.10	524.3	4.2
RIDN99-27.1i	93	68	0.73	2	0.0607	0.0028	11.22	0.25	549.2	11.7
RIDN99-28.1	75	47	0.63	4	0.0587	0.0026	10.80	0.18	571.3	9.3
RIDN99-29.1	268	135	0.51	0	0.0597	0.0013	11.53	0.18	535.9	7.9
RIDN99-30.1	125	94	0.76	1	0.0608	0.0012	11.46	0.16	538.2	7.2
RIDN99-31.1	101	88	0.87	0	0.0606	0.0017	11.38	0.27	542.2	12.4
RIDN99-32.1	692	742	1.07	70	0.0862	0.0010	13.28	0.16	453.1	5.3
RIDN99-33.1	163	102	0.62	1	0.0586	0.0011	10.84	0.16	569.1	8.2
RIDN99-34.1i	68	44	0.64	1	0.0627	0.0019	11.09	0.28	554.1	13.3
RIDN99-35.1i	117	69	0.59	1	0.0595	0.0016	11.00	0.17	560.8	8.6
RIDN99-36.1	169	194	1.15	3	0.0606	0.0009	10.68	0.20	575.9	10.5
RIDN99-37.1	110	62	0.57	2	0.0624	0.0014	11.36	0.18	541.8	8.1
RIDN99-39.1i	130	136	1.05	0	0.0595	0.0011	11.02	0.14	559.9	6.9
RIDN99-41.1	410	316	0.77	2	0.0588	0.0006	10.17	0.11	564.2	5.7
RIDN99-42.1	376	332	0.88	2	0.0595	0.0010	9.80	0.14	584.2	7.7
RIDN99-43.1i	293	317	1.08	3	0.0605	0.0007	10.15	0.19	564.2	10.1
RIDN99-44.1	191	90	0.47	0	0.0661	0.0011	11.14	0.19	512.5	8.4
RIDN99-45.1	204	104	0.51	3	0.0964	0.0007	3.58	0.03	1427.4	12.3
RIDN99-46.1i	140	101	0.72	5	0.0607	0.0014	10.30	0.17	556.0	8.9
RIDN99-47.1	347	5	0.01	1	0.0643	0.0011	7.72	0.08	728.7	6.8
RIDN99-48.1i	107	58	0.55	3	0.0616	0.0020	10.21	0.22	560.1	11.9
RIDN99-49.1	292	208	0.71	3	0.0609	0.0009	9.76	0.11	585.3	6.1
RIDN99-50.1	617	943	1.53	137	0.1248	0.0010	15.34	0.14	349.5	3.1

Weighted mean age at 2σ (n = 20, MSWD = 1.06) = 556 ± 1.6 Ma

Notes: MSWD = mean square of weighted deviates; i = sample included in preferred weighted mean age calculation; U-Pb constants by Steiger and Jäeger (1977)

[1] Concentrations of U and Th analyzed using the SHRIMP-RG

[2] Absolute counting errors (1σ)

[3] Error in millions of years

a result of reactions with diverse source rocks.

Neoproterozoic evolution

Galena, K-feldspar, and molybdenite, as a group, have a relatively narrow range of Pb isotope compositions, including the least radiogenic values from each of the deposits. Because of the lack of U and Th in galena, and because of the typically low U/Pb and Th/Pb values of K-feldspar these are interpreted to be close to the original ratios. In contrast to U- and Th-poor minerals, most pyrite, chalcopyrite, and sphalerite, in addition to sericite, have large isotopic ranges, even within individual deposits (App., Fig. 9).

Lines illustrating the trends for galena and feldspar (Fig. 10) have steep slopes and are thought to represent the original reservoir mixtures in each of the deposits, from less radiogenic (mantlelike) to more radiogenic compositions (crustal). A relatively unradiogenic end-member composition can be se-

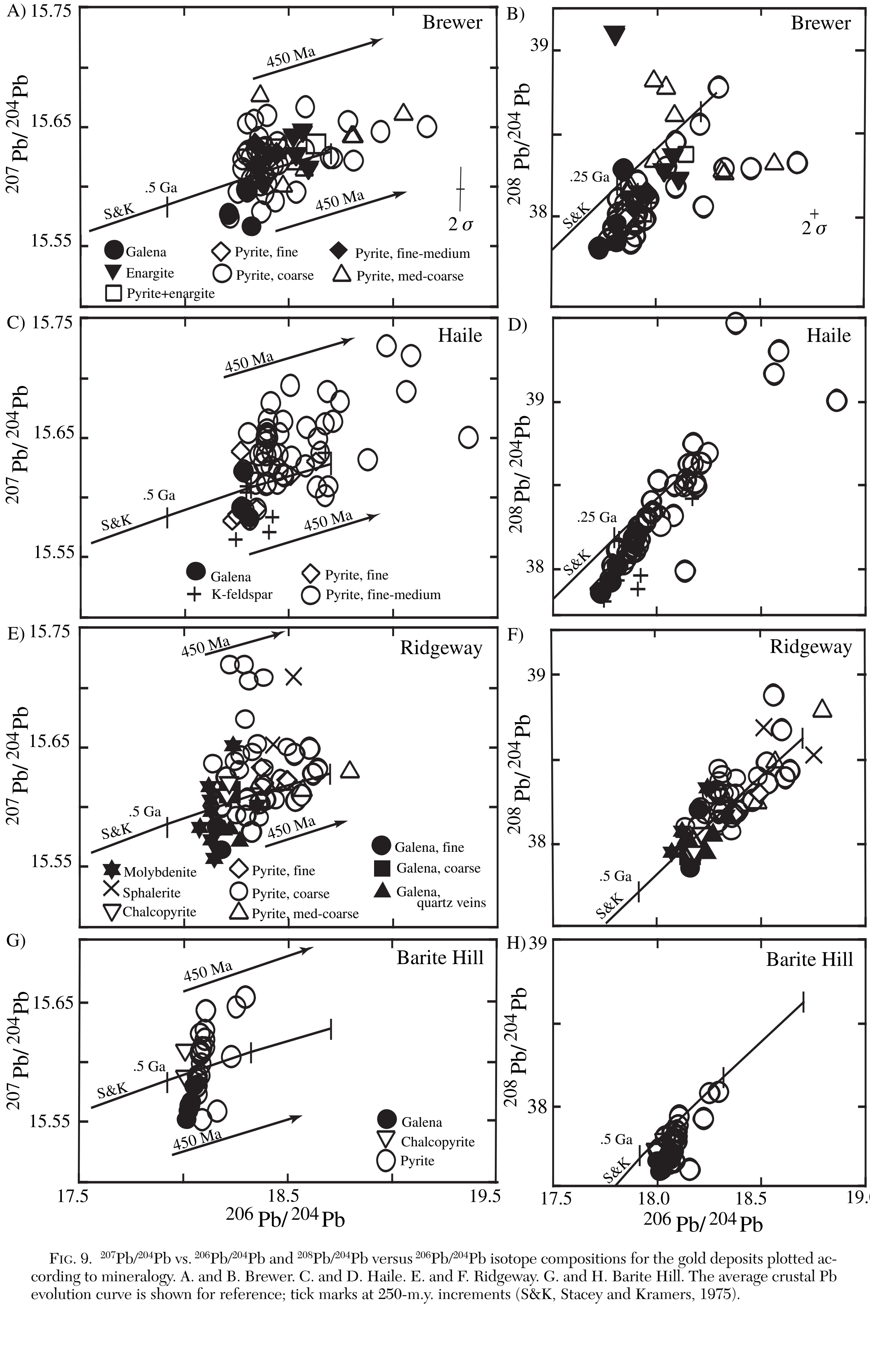

FIG. 9. $^{207}Pb/^{204}Pb$ vs. $^{206}Pb/^{204}Pb$ and $^{208}Pb/^{204}Pb$ versus $^{206}Pb/^{204}Pb$ isotope compositions for the gold deposits plotted according to mineralogy. A. and B. Brewer. C. and D. Haile. E. and F. Ridgeway. G. and H. Barite Hill. The average crustal Pb evolution curve is shown for reference; tick marks at 250-m.y. increments (S&K, Stacey and Kramers, 1975).

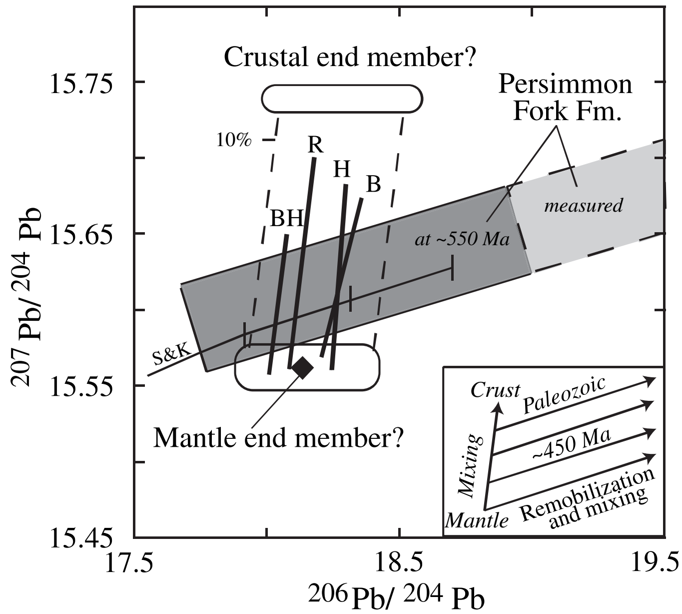

FIG. 10. Plot of $^{207}Pb/^{204}Pb$ vs. $^{206}Pb/^{204}Pb$ illustrating possible sources of Pb. Heavy lines depict the estimated best-fit trend of initial isotopic compositions, derived mostly from galena and K-feldspar, as a result of mixing of an upper crust end member and a less radiogenic end member. Field for the Persimmon Fork Formation has been age corrected to 550 Ma, using measured U, Th, and Pb concentrations (R. Ayuso, unpub. data). Estimated composition of the mantle in South Carolina shown as black diamond ($^{206}Pb/^{204}Pb$ = 18.15, $^{207}Pb/^{204}Pb$ = 15.57, $^{208}Pb/^{204}Pb$ = 37.80; LeHuray, 1987). Mixing calculations suggest less than 10% from the crustal end member is needed to satsify the inferred initial compositions. Inset shows approximate slopes at 450 Ma for reference. Average crustal Pb evolution curve as in Figure 9.

lected for the Persimmon Fork Formation, approximating that of the mantle and consistent with its Nd isotope signature (ε_{Nd} values as high as 4; Ayuso et al., 1998). Moreover, the least radiogenic age-corrected compositions of the Persimmon Fork Formation (Fig. 10), estimated using present-day U, Th, and Pb contents, roughly resemble the values proposed as Neoproterozoic mantle (LeHuray, 1987). More importantly, the age-corrected field substantially overlaps the isotopic trends of all but the highest $^{207}Pb/^{204}Pb$ values during the Neoproterozoic evolution of the sulfides (Fig. 10). If a small contribution from a more evolved reservoir were needed to explain the most radiogenic values, this hypothetical end member would have upper crustal compositions (Doe and Zartman, 1979) and be equivalent to old continental crust, or sedimentary rocks derived from such a crust. Simple mixing, at Barite Hill, for example, would have required a contribution of <10 percent from the proposed crustal rocks and >90 percent from the Persimmon Fork Formation.

Especially noteworthy in the slate belt gold deposits is the relative enrichment in $^{207}Pb/^{204}Pb$, suggesting a broad resemblance to sulfides from the Okinawa trough (Halbach et al., 1997) and Kuroko deposits in Japan (Doe and Zartman, 1982; Fehn et al., 1983; Fig. 11). Comparable high values of $^{207}Pb/^{204}Pb$ are also found in deposits from modern sedimented ridges (generally $^{207}Pb/^{204}Pb$ >15.55; Goodfellow and Zierenberg, 1999). However, most values of $^{208}Pb/^{204}Pb$ in the slate belt straddle or plot along the average crustal Pb model curve and generally are not enriched in $^{208}Pb/^{204}Pb$ relative to $^{206}Pb/^{204}Pb$ (except in some samples from the Ridgeway deposit; Fig. 9F). There is no clear evidence in the slate belt deposits for isotopic contributions from a rejuvenated continen-

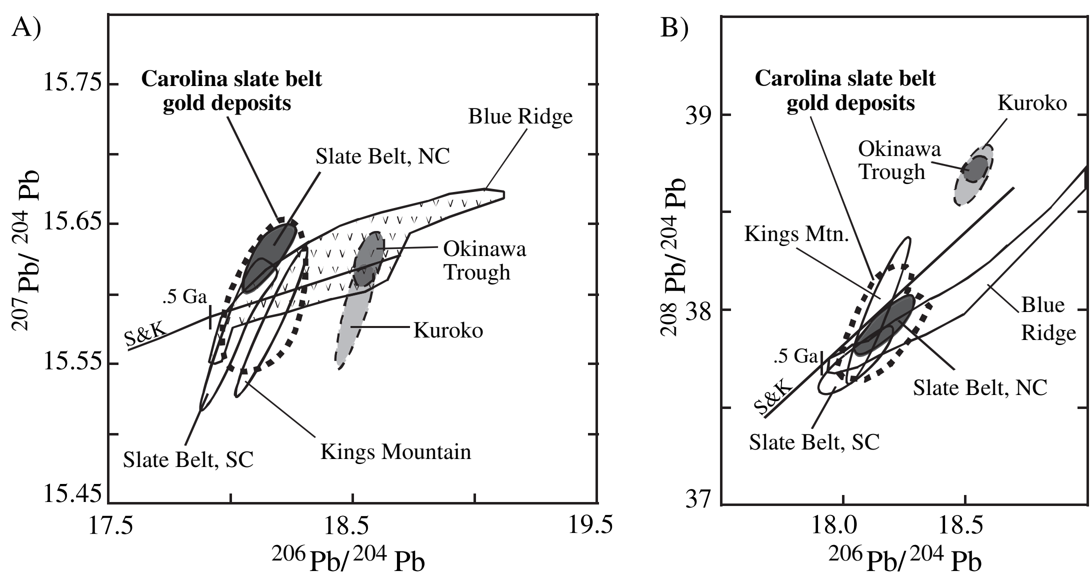

FIG. 11. Comparison of estimated initial isotopic compositions for the Carolina slate belt gold deposits (dashed line includes mostly galenas and K-feldspars) and volcanogenic massive sulfide deposits from the southern Appalachians. A. $^{207}Pb/^{204}Pb$ vs. $^{206}Pb/^{204}Pb$. B. $^{208}Pb/^{204}Pb$ vs. $^{206}Pb/^{204}Pb$. Galenas from Early to Middle Ordovician volcanogenic massive sulfide deposits from the slate belt in North Carolina (dark field, Kish and Feiss, 1982), and for massive sulfides from different provinces of the southern Appalachians, including the slate belt in South Carolina (stippled), Kings Mountain belt (cross hatch), and the Blue Ridge (Le Huray, 1982), which are shown for comparison. Also included are Pb isotope compositions for sulfides from Kuroko ores (Doe and Zartman, 1982; Fehn et al., 1983) and for the JADE hydrothermal field in the Okinawa trough (Halbach et al., 1997). Average crustal Pb evolution curve as in Figure 9.

tal craton, as may be the case for the Okinawa trough. The results also preclude associating the gold deposits to tectonic settings such as ocean ridges, primitive island arcs, or oceanic back arcs in the absence of a crustal source of Pb. The relatively high values of $^{207}Pb/^{204}Pb$ link the slate belt deposits to a continental margin and to contributions from isotopically evolved and older continental crust. This is consistent with the presence of inherited zircons in the Persimmon Fork Formation (up to about 1.8 Ga), together with the relatively old whole-rock Nd model ages (up to about 2 Ga; Ayuso et al., 1999; Fig. 9). The diversity in values of $^{207}Pb/^{204}Pb$ (but also in $^{206}Pb/^{204}Pb$ and $^{208}Pb/^{204}Pb$) in the deposits could be attributed to the influence of terrigenous sediments that evolved with high U/Pb and Th/Pb values. Such sediments would have been derived from the continental crust and supplied to local basins in a rifting or thinning continental lithosphere. Variable but decreasing influence of such isotopically evolved reservoirs may account for less radiogenic compositions from northern to southern South Carolina, in a trend from Brewer, Haile, Ridgeway, and Barite Hill. Oceanic crust and/or mantle-derived isotopic reservoirs were more important at Barite Hill, but in northern South Carolina thinned continental crust predominated.

Paleozoic evolution

The second stage of evolution of the deposits is likely represented by sulfides having higher $^{206}Pb/^{204}Pb$ and $^{207}Pb/^{204}Pb$ that depart from the steep slopes characterizing the Neoproterozoic evolution (Fig. 10). We interpret these isotopic values to represent a Paleozoic (?) stage of evolution that can be explained by in situ radiogenic Pb growth as a result of the U/Pb and Th/Pb evolution or from mixing with more radiogenic Pb. Possible sources of radiogenic Pb are seawater and buried crustal basements or from metasedimentary and metavolcanic rocks.

Simple in situ growth of radiogenic Pb is difficult to assess because the host rocks (especially those containing abundant sulfide minerals) were silicified and sericitized, intensely folded, and influenced by metal remobilization. Structural and mineralogical disturbances are likely to have strongly affected the original U, Th, and Pb concentrations, and present-day U/Pb values do not necessarily yield the original Pb isotope compositions. Moreover, U, Th, and Pb contents obtained from representative bulk sulfide samples indicate low present-day values of $^{238}U/^{204}Pb$ (<1.5) and $^{232}Th/^{204}Pb$ (<9.1). In situ evolution under these conditions cannot account for the entire range of observed Pb isotope compositions in the sulfides ($^{206}Pb/^{204}Pb$ and $^{207}Pb/^{204}Pb$ are too high). Although in situ growth of radiogenic Pb is likely to have contributed to the wide range of compositions, it is likely that the remobilized sulfides have incorporated radiogenic Pb. Also, the sulfides could have incorporated Pb from heated seawater, but estimates of water/rock ratios are unreasonably high and cannot be the main explanation for the high $^{207}Pb/^{204}Pb$ values.

Radiogenic Pb might also have been derived from the immediate host rocks or from an underlying sequence of older, deeper, and intensely altered radiogenic metavolcanic and metasedimentary rocks or older basement rocks (e.g., which provided the older, inherited $^{206}Pb/^{238}U$ spot ages in the zircons). Metavolcanic and metasedimentary rocks hosting the deposits plot as a large isotopic field that overlaps the values associated with remobilized sulfides in the deposits (high $^{206}Pb/^{204}Pb$ and $^{207}Pb/^{204}Pb$ values, Fig. 10). This overlap is consistent with rock-fluid reactions that leached Pb from these rocks (~450 Ma?) and were contributed to the sulfide minerals, in addition to the contributions of in situ growth of Pb (Fig. 10). Although the Persimmon Fork Formation appears to fullfill the requirements indicated above, we could not eliminate a contribution from older crustal basement rocks. However, the nature of the crust underlying the Carolina terrane is uncertain. Two types of basements are possible, Grenville or Gondwanan. Although neither basement is exposed in South Carolina (Secor et al., 1983), in the following section we generally assess the contributions of the nearest basements to the gold deposits.

Grenville massifs, peri-Gondwanan terranes, and the slate belt gold deposits

The Middle Cambrian magmatic arc in North Carolina is interpreted as having a Grenville-type crustal root (Mueller et al., 1996), consistent with a genetic connection to Laurentia (Samson et al., 1990). The arc includes rocks with values of $^{207}Pb/^{204}Pb$ (<15.48; Samson, 1995; Wortman et al., 2000) that are too low to match the compositions of sulfides from gold deposits of South Carolina ($^{207}Pb/^{204}Pb$ >15.55). Grenville-type basement in North Carolina, representing the nearest basement massifs, also has lower values of $^{207}Pb/^{204}Pb$ (Sinha et al., 1994) than the most radiogenic sulfides in the gold deposits (Fig. 12).

The North Carolina portion of the Carolina terrane contains two contrasting age and chemical groups of metavolcanic rocks (Hibbard and Samson, 1995). An older sequence (ca. 650–600 Ma) was built on oceanic crust and was derived mainly from juvenile and mantle sources (Samson, 1995; Samson et al., 1995; Fullagar et al., 1997; Wortman et al., 2000). The younger metavolcanic rocks (ca. 570–540 Ma), which contain broadly correlative rocks as those in the Persimmon Fork Formation of South Carolina, indicate a mature arc or back-arc environment (e.g., Feiss, 1982; Rogers, 1982; Feiss et al., 1993). Volcanic rocks in North Carolina that are broadly correlative to the Persimmon Fork Formation are thought to have been influenced by Grenville-type crust on the basis of xenocrystic zircons having minimum U-Pb ages of about 1.23 Ga and whole rocks with old Nd model ages (about 1.55 Ga) and ε_{Nd} values about +2.3 to –0.7 (Mueller et al., 1996). Our studies have shown that the Persimmon Fork Formation in South Carolina also incorporated crustal contributions, but a discrete xenocrystic zircon population that compellingly points to Grenville-type crust has not been identified. However, Pb isotope differences are sufficient to suggest that the Grenville massifs cannot generate the entire range of isotopic compositions observed in the sulfides by simple leaching and that they probably do not represent the radiogenic source controlling the high $^{207}Pb/^{204}Pb$ values. This result may also apply to volcanogenic massive sulfide deposits in the Carolina terrane and from various geologic provinces in the southern Appalachians (Kish and Feiss, 1982; LeHuray, 1982) that have ages that are broadly similar (Proterozoic to Middle Ordovician) to the gold deposits. Notably all of these

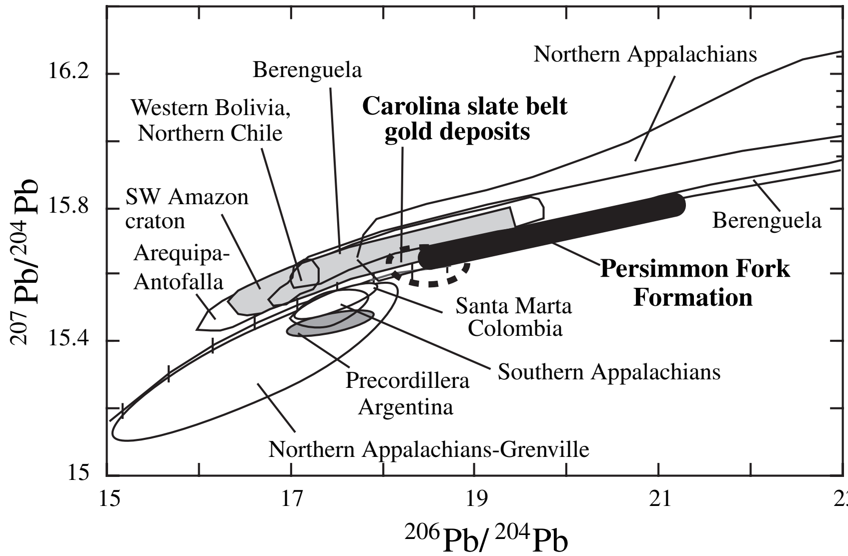

FIG. 12. Plot of initial $^{207}Pb/^{204}Pb$ vs. $^{206}Pb/^{204}Pb$ for volcanic rocks hosting the Carolina slate belt deposits and basement rocks from the northern Appalachians. Also, shown are isotopic fields for the Grenville (Vermont, Ontario, and Cape Breton Island). Sources of data include: Ayuso and Bevier (1991), R.A. Ayuso and N. Ratcliffe (unpub. data), DeWolffe and Mezger (1994), Ayuso et al. (1996), and Whalen et al. (1997, and references therein). The southern Appalachians are represented by basement rocks from Tallulah Falls, Pine Mountain, and Corbin Gneiss in Georgia, and Sauratown Mountains in North Carolina. Source of data: Sinha et al. (1994). Data for the South American basements are from Tosdal (1996), Tosdal et al. (1994, and references therein), Murphy et al. (1999, and references therein). Average crustal Pb evolution curve as in Figure 9.

volcanogenic massive sulfide deposits have isotopic compositions that overlap (Fig. 11).

Deposits having equivalent age and metallogeny to the gold deposits in the Carolina terrane can be found in Maritime Canada (e.g., Huard and O'Driscoll, 1986) within the Avalonian tectonic zone. Together with various other terranes (e.g., Cadomia, West Avalonia, East Avalonia), all were peripheral to Gondwana during the Late Proterozoic to Early Ordovician. Moreover, lithologic and geochemical similarities between the Carolina terrane and Cadomian terranes in western (Dennis and Shervais, 1996; Nance and Murphy, 1996) and central Europe have been noted (Samson et al., 1990), but exact age (see summary by Bierlein and Crowe, 2000, and references therein), metallogenic, and isotopic analogues to the Neoproterozoic, volcanic-related, pyritic gold deposits in the Carolina slate belt appear uncommon in the Cadomian terranes. Correlations among the peri-Gondwanan terranes and adjacent cratonal blocks (Baltica, Amazonian, and West African) remain controversial, but recent studies suggest that the peri-Gondwanan terranes were located along the northern flank of present-day South America and northwestern Africa (Nance and Murphy, 1996; Murphy et al., 1999). Pb isotope compositions of Avalonian igneous and metamorphic rocks in the northern Appalachians and our new data for the Persimmon Fork Formation in the Carolina terrane support a broad correlation with South American basements (Fig. 12). However, exact metallogenic or isotopic analogues to the slate belt gold deposits of South Carolina have not yet been recognized in South America or in other peri-Gondwanan cratonal blocks.

Summary and Conclusions

Volcanic rocks of the Persimmon Fork Formation dated by zircon U-Pb (SHRIMP-RG) geochronology indicate the following ages for host rocks of the largest gold-pyrite-sericite deposits of the Carolina slate belt: 550 ± 3 Ma for Brewer, 553 ± 2 Ma for Haile, and 556 ± 2 Ma for the Ridgeway deposit. Pb isotope compositions of sulfide and silicate minerals for Brewer, Haile, Ridgeway, and Barite Hill straddle the average crustal Pb growth curve and link the deposits to isotopically evolved rocks. The Persimmon Fork Formation is the dominant source of Pb in the deposits. Sulfides from Barite Hill (e.g., galena $^{206}Pb/^{204}Pb$ <18.077) in southern South Carolina are less radiogenic than sulfides from Ridgeway ($^{206}Pb/^{204}Pb$ >18.169), Haile ($^{206}Pb/^{204}Pb$ >18.233), and Brewer ($^{206}Pb/^{204}Pb$ >18.311) in northern South Carolina. Geologic and Pb isotope data support genetic links to a shallow submarine environment where pyrite-gold-silica mineralization was concentrated in intrusive breccias, stockwork veining, layered disseminations, and subaerial and submarine hot springs, with increasing crustal contribution of Pb from south to north. In this respect, the deposits have a broad resemblance to the metallogenic evolution of sulfide deposits in the Okinawa trough and the Hokuroku district in Japan. Diversity in $^{206}Pb/^{204}Pb$ and $^{207}Pb/^{204}Pb$ in the deposits requires input of crustal rocks and/or terrigenous sediments supplied to local basins in a rifting or thinning continental lithosphere. Oceanic crust or mantle-derived isotopic reservoirs were more important at Barite Hill than in northern South Carolina where thinned continental crust predominated. The isotopic composition of Pb in basement rocks from Grenville-type massifs and in sulfides from the South Carolina gold deposits do not match. A direct genetic link between Grenville basement and the gold deposits is unlikely. Gold deposits in the Carolina slate belt share broadly similar age and metallogenic features with deposits from the Avalonian terrane in Maritime Canada and may share a similar source of Pb.

Acknowledgments

We thank John Scheetz and Mark Zwaschka from the Brewer mine (Brewer Gold), Tom Kilbey and John Maddry from the Haile mine (AMAX Gold, Piedmont Mining), Langdon Mitchell and Ken Gillon from the Ridgeway mine (Kennecott Ridgeway Mining Company), and Dennis LaPoint (Appalachian Resources) for providing support in the field, access to the mines, and data. We benefited from discussions with colleagues from the U.S. Geologiical Survey, including S.H.B. Clark, C.G. Cunningham, T.L. Klein, R. Koeppen, and T. Offield on the genesis of the gold deposits. Appreciation is expressed to C. Coath for his help in the ion microprobe lab at the University of California, Los Angeles, H. Persing in the SHRIMP lab, G. Wandless, A. Paone, and R. Somma for their help in the U.S. Geological Survey radiogenic isotope lab, and to J. Jackson and A. Lyon for their contributions in the mineral separation lab. An earlier version of this paper benefited from detailed reviews by Bruce Doe and Wright Horton (both at the U.S. Geological Survey). We thank B. Dubè, W. Premo, R. Tosdal, and M. Hannington for detailed reviews and helpful comments to improve the manuscript.

May 23, 2002; December 16, 2004

REFERENCES

Ayuso, R.A. and Bevier, M.L., 1991, Regional differences in Pb isotopic compositions of feldspars in plutonic rocks of the northern Appalachian Mountains, U.S.A. and Canada: A geochemical method of terrane correlation: Tectonics, v. 10, p. 191–212.

Ayuso, R.A., Barr, S.M., and Longstaffe, F.J., 1996, Pb and O isotopic constraints on the source of granitic rocks from Cape Breton Island, Nova Scotia, Canada: American Journal of Science, v. 296, p. 789–817.

Ayuso, R.A., Foley, N.K., Seal, R.R., II, Offield, T., and Kunk, M.J., 1997, Genesis of gold deposits in the Carolina slate belt, USA: Regional constraints from trace element, Pb, and Nd isotopic variations and Ar-Ar ages [abs.]: Geological Society of America Abstracts with Programs, v. 29, p. A-60.

Ayuso, R.A., Foley, N.K., Seal, R.R., II, and Offield, T., 1998, Genesis of gold deposits in the Carolina slate belt, USA [abs.]: Constraints from comparative mineralogy, trace elements, fluid evolution, and isotopic variations: Symposium Geology II Circum Atlantic Mineral Deposits: The North Atlantic, Society of Mining, Metallurgy, and Exploration, SME Annual Meeting, Orlando, Florida, Abstracts, p. 62.

Ayuso, R.A., Sinha, A.K., Seal, R.R., Foley, N.K., and Offield, T.O., 1999, Gold deposits of the Carolina slate belt: Zircon geochronology and isotopic characteristics [abs.]: Geological Society of America Abstracts with Programs, v. 31, p. A-3.

Ayuso, R.A., Wooden, J.N., Foley, N.K., Slack, J.F., Sinha, A.K., and Persing, H., 2003, Pb isotope geochemistry and zircon (SHRIMP-RG ion microprobe) age of the Bald Mountain deposit, northern Maine: Ordovician massive sulfide product of mantle and crustal contributions: ECONOMIC GEOLOGY MONOGRAPH 11, p. 589–609.

Bacon, C.R., Persing, H.M., Wooden, J.L., and Ireland, T.R., 2000, Late Pleistocene granodiorite beneath Crater Lake caldera, Oregon, dated by ion microprobe: Geology, v. 28, p. 467–470.

Barker, C.A., Secor, D.T., Pray, J.R., and Wright, J.E., 1998, Age and deformation of the Longtown metagranites, South Carolina Piedmont: A possible constraint on the origin of the Carolina terrane: Journal of Geology, v. 106, p. 711–723.

Bierlein, F.P., and Crowe, D.E., 2000, Phanerozoic orogenic lode gold deposits: Reviews in Economic Geology, v. 13, p. 103–139.

Butler, J.R., and Secor, D.T., 1991, The Central Piedmont: Carolina Geological Society Fiftieth Anniversary Volume, p. 59–78.

Carpenter, R.H., Odom, A.L., and Hartley, M.E., III, 1982, Geochronological investigation of the Lincolnton metadacite, Georgia and South Carolina: Geological Society of America Special Paper 191, p. 145–152.

Clark, S.H.B., Gray, K.J., and Back, J.M., 1999, Geology of the Barite Hill gold-silver deposit in the southern Carolina slate belt: ECONOMIC GEOLOGY, v. 94, p. 1329–1346.

Cumming, G.L., and Richards, J.R., 1975, Ore lead isotope ratios in a continuously changing Earth: Earth and Planetary Science Letters, v. 28, p. 155–171.

Dennis, A.J., 1995, The Carolina terrane in northwestern South Carolina: Relative timing of events and recent tectonic models: Geological Association of Canada Special Paper 41, p. 173–190.

Dennis, A.J., and Shervais, J.W., 1996, The Carolina terrane in northwestern South Carolina: Insights into the development of an evolving island arc: Geological Society of America Special Paper 304, p. 237–256.

DeWolfe, C.P., and Mezger, K., 1994, Lead isotope analyses of leached feldspars: Constraints on the early history of the Grenville orogen: Geochimica et Cosmochimica Acta, v. 58, p. 5537–5550.

Doe, B.R., and Zartman, R.E., 1979, Plumbotectonics I: the Phanerozoic, *in* Barnes, H., ed., Geochemistry of hydrothermal ore deposits, 2nd ed.: New York, John Wiley, p. 22–70.

——1982, Plumbotectonics of Japan: Some evidence for a rejuvenated craton: Mining Geology, v. 32, p. 285–289.

Dubè, B., Dunning G., and Lauziere, K., 1998, Geology of the Hope Brook mine, Newfoundland, Canada: A preserved Late Proterozoic high-sulfidation epithermal gold deposit and its implications for exploration: ECONOMIC GEOLOGY, v. 93, p. 405–436.

Duckett, R.P., Evans, P.H., and Gillon, K.A., 1988, Economic geology of the Ridgeway gold deposits, Fairfield County, South Carolina, *in* Secor, D.T., Jr., ed., Southeastern geological excursions: South Carolina Geological Survey, Geological Society of America, Southeastern Section, Field trip guidebook, p. 40–45.

Eager, W.G., Crowe, D.E., and Mitchell, T.L., 1997, Geology and stable isotope geochemistry of the Ridgeway North pit deposit, Ridgeway, S.C.: Evidence for a syngenetic origin [abs.]: Geological Society of America Abstracts with Programs, v. 29, p. 15.

Fehn, U., Doe, B.R., and Delevaux, M.H., 1983, The distribution of lead isotopes and the origin of Kuroko ore deposits in the Hokuroku district, Japan: ECONOMIC GEOLOGY MONOGRAPH 5, p. 488–506.

Feiss, P.G., 1982, Geochemistry and tectonic setting of the volcanics of the Carolina slate belt: ECONOMIC GEOLOGY, v. 77, p. 273–293.

Feiss, G., and Slack, J.F., 1989, Mineral deposits of the U.S. Appalachians: Geological Society of America, Geology of North America, v. F-2, p. 471–494.

Feiss, P.G., Vance, R.K., and Weslowski, D.J., 1993, Volcanic rock-hosted gold and base-metal mineralization associated with Neoproterozoic-Early Paleozoic back-arc extension in the Carolina terrane, southern Appalachian Piedmont: Geology, v. 21, p. 439–442.

Foley, N.K., Ayuso, R.A., Seal, R.R., II, and Offield, T.W., 1997, Fluid evolution and mineralogy of Au-bearing volcanogenic deposits in a regional geologic setting: Examples from the Carolina slate belt, USA [abs.]: Geological Society of America Abstracts with Programs, v. 29, p. A-59.

Foley, N.K., Ayuso, R.A., and Seal, R.R., 2001, Remnant colloform pyrite at the Haile gold deposit, South Carolina: A textural key to genesis: ECONOMIC GEOLOGY, v. 96, p. 891–902.

Fullagar, P.D., 1981, Summary of Rb-Sr whole-rock ages for South Carolina: South Carolina Geology, v. 25, p. 29–32.

Fullagar, P.D., Goldberg, S.A., and Butler, J.R., 1987, Rb-Sr ages of metavolcanic rocks from the Carolina and Eastern slate belts of North and South Carolina [abs.]: Geological Society of America Abstracts with Programs, v. 19, p. 84.

——1997, Nd and Sr isotopic characterization of crystalline rocks from the southern Appalachian Piedmont and Blue Ridge, North and South Carolina: Geological Society of America Memoir 191, p. 165–180.

Gillon, K.A., Spence, W.H., Duckett, R.P., and Benson, C.J., 1995, Geology of the Ridgeway gold deposits, Ridgeway, South Carolina: Society of Economic Geologists Guidebook Series, v. 24, p. 53–94.

Gillon, K.A., Mitchell, T.L., Dinkowitz, S.R., Barnett, R.L., 1998 for 1997, The Ridgeway gold deposits: A window to the evolution of a Neoproterozoic intra-arc basin in the Carolina terrane, South Carolina: South Carolina Geology, v. 40, p. 29–70.

Goodfellow, W.D., and Zierenberg, R.A., 1999, Genesis of massive sulfide deposits at sediment-covered spreading centers: Reviews in Economic Geology, v. 8, p. 297–324.

Halbach, P., Hansman, W., Koppel, V., and Pracejus, B., 1997, Whole-rock and sulfide lead-isotope data from the hydrothermal JADE field in the Okinawa back-arc trough: Mineralium Deposita, v. 32, p. 70–78.

Hannington, M.D., Poulsen, K.H., Thompson, J.F.H., and Sillitoe, R.H., 1999, Volcanogenic gold in the massive sulfide environment: Reviews in Economic Geology, v. 8, p. 325–356.

Hardy, L.S., 1989, Hydrothermal potassium feldspar at the Haile gold mine, South Carolina: ECONOMIC GEOLOGY, v. 84, p. 2307–2310.

Hayward, N., 1992, Controls on syntectonic replacement mineralization in parasitic antiforms, Haile gold mine, Carolina slate belt: ECONOMIC GEOLOGY, v. 87, p. 91–112.

Hibbard, J.P., and Samson, S.D., 1995, Orogenesis exotic to the Iapetan cycle in the southern Appalachians: Geological Association of Canada Special Paper 41, p. 191–205.

Horton, J.W., Drake, A.A., and Rankin, D.W., 1989, Tectonostratigraphic terranes and their Paleozoic boundaries in the central and southern Appalachians: Geological Society of America Special Paper 230, p. 213–245.

Huard, A., and O'Driscoll, C.F., 1986, Epithermal mineralization in Late Precambrian volcanic rocks of the Burin peninsula: Current Research, Newfoundland Department of Mines, Energy, Mineral Development Division Report 86-1, p. 65–78.

Ireland, T.R., 1994, Ion microprobe mass spectrometry: Techniques and applications, *in* Hyman, M., and Rowe, M., eds., Cosmochemistry, geochemistry, and geochronology: Advances in Analytical Geochemistry: JAI Press, p. 1–118.

Kiff, I.T., and Spence, W.H., 1987, Volcanogenic-epithermal-exhalative gold deposits of the Haile-type in the Carolina slate belt [abs.]: Geological Society of America Abstracts with Programs, v. 19, p. 394.

Kish, S.A., and Feiss, G., 1982, Application of lead isotope studies to massive sulfide and vein deposits of the Carolina slate belt: ECONOMIC GEOLOGY, v. 77, p. 352–363.

LeHuray, A.P., 1982, Lead isotope patterns of galena in Piedmont and Blue Ridge deposits, southern Appalachians: ECONOMIC GEOLOGY, v. 77, p. 335–351.

——1987, U-Pb and Th-Pb whole rock isochrons from metavolcanic rocks of the Carolina slate belt: Geological Society of America Bulletin, v. 99, p. 354–361.

Ludwig, K.R., 1999, Isoplot/Ex version 2.01—geochronological toolkit for Microsoft Excel: Berkley Geochronology Center Special Publication 1a, 47 p.

Maddry, J.W., and Kilbey, T.R., 1995, Geology of the Haile gold mine: Society of Economic Geologists Guidebook Series, v. 24, p. 147–172.

McSween, H.Y, Speer, J.A., and Fullagar, P.D., 1991, Plutonic rocks, *in* Horton, J.W., Jr., and Zullo, V.A., eds., The geology of the Carolinas: Knoxville, University of Tennessee Press, p. 109–126.

Mueller, P.A., Kozuch, M., Heatherington, A.L., Wooden, J.W., Offield, T.O., Koeppen, R.K., Klein, T.L., and Nutman, A.P., 1996, Evidence for Mesoproterozoic basement in the Carolina terrane and speculation on its origin: Geological Society of America Special Paper 304, p. 207–217.

Murphy, J.B., Keppie, J.D., Dostal, J., and Nance, R.D., 1999, Neoproterozoic-Early Paleozoic evolution of Avalonia: Geological Society of America Special Paper 336, p. 253–265.

Nance, R.D., and Murphy, J.B., 1996, Basement isotopic signatures and Neoproterozoic paleogeography of Avalonian-Cadomian and related terranes in the circum North Atlantic: Geological Society of America Special Paper 304, p. 333–346.

O'Brien, S.J., Dubé, B., O'Driscoll, C.F., and Mills, J., 1998, Geological setting of gold mineralization and related hydrothermal alteration in Late Neoproterozoic (post-640 Ma) Avalonian rocks of Newfoundland, with a review of coeval gold deposits elsewhere in the Appalachian Avalonian belt: Current Research (1998) Newfoundland Department of Mines and Energy Geological Survey Report 98-1, p. 93–124.

O'Brien, S.J., Dubé, B., and O'Driscoll, C.F., 2001, Epithermal-style hydrothermal systems in Late Neoproterozoic Avalonian rocks on the Avalon peninsula, Newfoundland: Implications for gold exploration: Geological Association of Canada-Mineralogical Association of Canada Annual Meeting, St John's, Newfoundland, May 27–30, 2001, Field trip guidebook A6, 29 p.

Offield, T.W., 1994, Lithotectonic map and field data—reconaissance geology of the Carolina slate belt and adjacent rocks from southern Virginia to central South Carolina: U.S. Geological Survey Open-File Report 94-420, 58 p.

Paces, J.B., and Miller, J.D., 1993, U-Pb ages of Duluth Complex and related mafic intrusions, northeastern Minnesota: Geochronological insights to physical, petrogenetic, paleomagnetic, and tectomagmatic processes associated with the 1.1 Ga mid-continent rift system: Journal of Geophysical Research, v. 98, p. 13997–14013.

Pardee, J.R., and Park, C.F., Jr., 1948, Gold deposits of the southern Piedmont: U.S. Geological Survey Professional Paper 213, 156 p.

Richards, J.P., and Noble, S.R., 1998, Application of radiogenic isotope systems to the timing and origin of hydrothermal processesy: Reviews in Economic Geology, v. 10, p. 195–234.

Robert, F., Poulsen, K.H., and Dubé, B., 1997, Gold deposits and their geological classification: Exploration 97, International Conference on Mineral Exploration, 4th decennial, Toronto, GEO/FX, Proceedings, p. 209–220.

Rogers, J.J.W., 1982, Criteria for recognizing environments of formation of volcanic suites in the Carolina slate belt: Geological Society of America Special Paper 191, p. 99–107.

Sambridge, M.S., and Compston, W., 1994, Mixture modeling of multi-component data sets with application to ion-probe zircon ages: Earth and Planetary Sciences Letters, v. 128, p. 373–390.

Samson, S.D., 1995, Is the Carolina terrane part of Avalon?: Geological Association of Canada Special Paper 41, p. 253–266.

Samson, S.D., Palmer, A.R., Robison, R.A., and Secor, D.T., Jr., 1990, Biogeographical significance of Cambrian trilobites from the Carolina slate belt: Geological Society of America Bulletin, v. 102, p. 1459–1470.

Samson, S.D., Hibbard, J.P., and Wortman, G.L., 1995, Nd isotopic evidence for juvenile crust in the Carolina terrane, southern Appalachians: Contributions to Mineralogy and Petrology, v. 121, p. 171–184.

Scheetz, J.W., 1991, The geology and alteration of the Brewer gold mine in South Carolina: Unpublished M.S. thesis, Chapel Hill, University of North Carolina, 180 p.

Seal, R.R., II, Ayuso, R.A., Foley, N.K., and Clark, S.H.B., 2001, Sulfur and lead isotope geochemistry of hypogene mineralization at the Barite Hill gold deposit, Carolina slate belt, southeastern United States: A window into and through regional metamorphism: Mineralium Deposita, v. 36, p. 137–148.

Secor, D.T., Samson, S., Snoke, A., and Palmer, P., 1983, Confirmation of the Carolina slate belt as an exotic terrane: Science, v. 221, p. 649–651.

Shervais, J.W., Shelley, S.A., and Secor, D.T., Jr., 1996, Geochemistry of the volcanic rocks of the Carolina and Augusta terranes in central South Carolina: An exotic rifted volcanic arc: Geological Society of America Special Paper 304, p. 219–236.

Sillitoe, R.H., 1991, Intrusion related gold deposits, *in* Foster, R.P., ed., Gold metallogeny and exploration: London, Blackie and Son, p. 165–209.

Sinha, A.K., Hogan, J.P., and Parks, J., 1994, Lead isotope mapping of crustal reservoirs within the Grenville Superterrane: I. Central and Southern Appalachians: Geophysical Monograph 95, p. 293–305.

Speer, W.E., and Maddry, J.W., 1993, Geology and recent discoveries at the Haile gold mine, Lancaster County, South Carolina: South Carolina Geology, v. 35, p. 9–26.

Spence, W.H., Worthington, J.E., Jones, E.M., and Kiff, I.T., 1980, Origin of the gold mineralization at the Haile mine in Lancaster County, South Carolina: Mining Engineering, v. 32, p. 70–73.

Stacey, J.S., and Kramers, J.D., 1975, Approximation of terrestrial lead isotope evolution by a two-stage model: Earth and Planetary Science Letters, v. 26, p. 207–222.

Steiger, R.H., and Jager, E., 1977, Subcommission on geochronology, convention on the use of decay constants in geo- and cosmochronology: Earth and Planetary Science Letters, v. 36, p. 359–362.

Stein, H.J., Markey, R.J., Morgan, J.W., Hannah, J.L., Zak, K., and Sundblad, K., 1997, Re-Os dating of shear-hosted Au deposits using molybdenite, *in* Papunen, H., ed.: Mineral deposits: research and exploration where do they meet?: Rotterdam, Balkema, p. 313–317.

Tera, F., and Wasserburg, G.J., 1972, U-Th-Pb systematics in three Apollo 14 basalts and the problem of initial Pb in lunar rocks: Earth and Planetary Science Letters, v. 14, p. 281–304.

Tomkinson, M.J., 1988, Gold mineralization in phyllonites at the Haile mine, South Carolina: ECONOMIC GEOLOGY, v. 83, p. 1392–1400.

Tosdal, R.M., 1996, Amazonia-Laurentia connection as viewed from the Middle Proterozoic basement of western Bolivia and northern Chile: Tectonics, v. 15, p. 827–842.

Tosdal, R.M., Munizaga, F., Williams, W.C., and Bettencourt, J.S., 1994, Middle Proterozoic crystalline basement in the central Andes, western Bolivia, and northern Chile: A U-Pb and Pb-Pb perspective [abs.]: Congreso Geologico Chileno, 7th, 1994, Universidad de Concepcion Actas, v. II, p. 1464–1467.

Whalen, J.B., van Staal, C.R., Longstaffe, F.J., Gariepy, C., and Jenner, G., 1997, Insights into tectonostratigraphic zone identification in southwestern Newfoundland based on isotopic (Nd, O, Pb) and geochemical data: Atlantic Geology, v. 33, p. 231–241.

Whitney, J.A., Paris, T.A., Carpenter, R.H., and Hartley, M.E., III, 1978, Volcanic evolution of the southern slate belt of Georgia and South Carolina: A primitive oceanic island arc: Journal of Geology, v. 86, p. 173–192.

Williams, H., and Hatcher, R.D., 1982, Suspect terranes and accretionary history of the Appalachian orogen: Geology, v. 10, p. 530–536.

Williams, I.S., 1996, U-Th-Pb geochronology by ion microprobe: Reviews in Economic Geology, v. 7, p. 1–36.

Worthington, J.E., 1993, The Carolina slate belt and its gold deposits: Reflections after a quarter century: South Carolina Geology, v. 35, p. 1–8.

Worthington, J.E., and Kiff, I.T., 1970, A suggested volcanogenic origin for certain gold deposits in the slate belt of the Carolina piedmont: ECONOMIC GEOLOGY, v. 65, p. 529–537.

Wortman, G.L., Samson, S.D., and Hibbard, J.P., 2000, Precise U-Pb zircon constraints on the earliest magmatic history of the Carolina terrane: Journal of Geology, v. 108, p. 321–338.

Zwaschka, M., and Scheetz, J.W., 1995, Detailed mine geology of the Brewer gold mine, Jefferson County, South Carolina: Society of Economic Geolo-

APPENDIX

Lead Isotope Compositions of Sulfide and Silicate Minerals from the Brewer, Haile, Ridgeway, and Barite Hill Gold Deposits of the Carolina Slate Belt, South Carolina

Sample	Split	$^{206}Pb/^{204}Pb$	$^{207}Pb/^{204}Pb$	$^{208}Pb/^{204}Pb$	Notes
Brewer					
Galena					
BDH8-189	Bulk	18.326	15.567	38.286	Main pit; fine- to medium-grained cubes
BDH118-71	Bulk	18.296	15.598	37.870	Main pit; fine- to medium-grained cubes, pyritic; in medium to coarse heterolithic breccia
BDH118-443a	Bulk	18.211	15.578	37.820	Main pit; fine-grained cubes, pyritic, with enargite; in fine to medium breccia
BDH118-443b	Bulk	18.217	15.575	37.793	Main pit; fine-grained cubes, pyritic, with enargite; in fine to medium breccia
Pyrite					
BDH2-58a	Leach 1	18.578	15.631	38.179	Main pit; sulfide-rich breccia, with hematite
BDH2-58b	Leach 2	18.357	15.641	38.009	Main pit; sulfide-rich breccia, with hematite
BDH2-58c	Residue	18.356	15.608	37.932	Main pit; sulfide-rich breccia, with hematite
BDH2-81a	Leach	18.809	15.622	38.289	Main pit; vuggy, fractured sulfide-rich breccia; with quartz and sericite
BDH2-81b	Residue	19.160	15.651	38.328	Main pit; vuggy, fractured sulfide-rich breccia; with quartz and sericite
BDH8-193a	Leach	18.432	15.588	37.994	Main pit; heterolithic breccia
BDH8-193b	Residue	18.363	15.602	37.846	Main pit; heterolithic breccia
BDH8-193c	Bulk	18.451	15.620	38.108	Main pit; heterolithic breccia
BDH8-193d	Bulk	18.382	15.633	37.960	Main pit; heterolithic breccia
BDH8-298a	Leach	18.318	15.625	37.967	Main pit; in medium to coarse heterolithic breccia
BDH8-298b	Residue	18.336	15.656	38.080	Main pit; in medium to coarse heterolithic breccia
BDH8-304.3a	Bulk	18.384	15.610	37.961	Main pit; in medium to coarse heterolithic breccia
BDH8-304.3b	Bulk	18.365	15.579	37.847	Main pit; in medium to coarse heterolithic breccia
BDH36-95a	Bulk	18.301	15.596	38.114	B6 pit; in medium to coarse breccia
BDH36-95b	Bulk	18.415	15.629	38.035	B6 pit; in medium to coarse breccia
BDH96-95c	Bulk	18.383	15.613	37.973	B6 pit; in medium to coarse breccia
BDH118-67.6a	Leach 1	18.446	15.628	38.133	Main pit; with enargite; in heterolithic breccia (quartz porphyry)
BDH118-67.6b	Leach 2	18.340	15.617	37.990	Main pit; with enargite; in heterolithic breccia (quartz porphyry)
BDH118-67.6c	Residue	18.336	15.635	38.023	Main pit; with enargite; in heterolithic breccia (quartz porphyry)
BDH118-71a	Leach	18.580	15.666	38.451	Main pit; with enargite; in medium to coarse heterolithic breccia
BDH118-71b	Residue	18.256	15.596	37.870	Main pit; with enargite; in medium to coarse heterolithic breccia
BDH118-75c	Leach 1	18.939	15.647	38.293	Main pit; with enargite; in heterolithic breccia (quartz porphyry clasts)
BDH118-75d	Leach 2	18.710	15.624	38.064	Main pit; with enargite; in heterolithic breccia (quartz porphyry clasts)
BDH118-75e	Residue	18.430	15.618	37.989	Main pit; with enargite; in heterolithic breccia (quartz porphyry clasts)
BDH118-334a	Leach 1	18.786	15.655	38.778	Main pit; heterolithic breccia (silica and felsic tuff clasts)
BDH118-334b	Leach 2	18.446	15.606	38.104	Main pit; heterolithic breccia (silica and felsic tuff clasts)
BDH118-334c	Residue	18.408	15.615	38.106	Main pit; heterolithic breccia (silica and felsic tuff clasts)
BDH118-386a	Leach	18.397	15.660	38.217	Main pit; with enargite; in heterolithic breccia (quartz porphyry clasts)
BDH118-386b	Residue	18.379	15.629	38.102	Main pit; with enargite; in heterolithic breccia (quartz porphyry clasts)
BDH118-386c	Leach	18.535	15.596	38.302	Main pit; with enargite; in heterolithic breccia (quartz porphyry clasts)
BDH118-386d	Residue	18.402	15.625	38.114	Main pit; with enargite; in heterolithic breccia (quartz porphyry clasts)
BDH118-443	Bulk	18.276	15.623	37.939	Main pit; with enargite; medium to coarse heterolithic breccia (quartz porphyry clasts)
BDH118-450a	Leach	18.693	15.625	38.552	Main pit; with quartz, sericite, and enargite; in pyrite-rich heterolithic breccia
BDH118-450b	Residue	18.347	15.630	38.049	Main pit; pyrite-rich heterolithic breccia; with quartz, sericite, and enargite
BDH118-450	Bulk	18.392	15.603	38.023	Main pit; pyrite-rich heterolithic breccia; with quartz, sericite, and enargite
BDH118-467	Bulk	18.630	15.636	38.369	Main pit; pyrite- and enargite-rich heterolithic breccia
BDH118-479	Bulk	18.438	15.631	38.146	Main pit; pyrite- and enargite-rich heterolithic breccia
BDH118-485	Bulk	18.367	15.632	38.097	Main pit; pyrite- and enargite-rich heterolithic breccia
BDH118-540	Bulk	18.307	15.630	37.960	Main pit; with abundant pyrite and aluminosilicates; in medium to coarse breccia
BDH119-185	Bulk	18.385	15.595	37.889	Main pit; with other sulfides and aluminosilicates; in heterolithic breccia
BDH119-227	Bulk	18.317	15.607	37.936	Main pit; with other sulfides and aluminosilicates; in heterolithic breccia
BDH119-232	Bulk	18.293	15.628	37.978	Main pit; with aluminosilicates and fine sulfides; in medium to coarse heterolithic breccia
BDH119-507	Bulk	18.298	15.653	38.021	Main pit; with very fine sulfides; in sericitic, aluminosilicate-bearing metatuff

APPENDIX (*Cont.*)

Sample	Split	$^{206}Pb/^{204}Pb$	$^{207}Pb/^{204}Pb$	$^{208}Pb/^{204}Pb$	Notes
BDH119-509	Bulk	18.280	15.615	37.921	Main pit; with very fine sulfides; in sericitic, aluminosilicate-bearing metatuff
BDH121-239a	Leach	18.474	15.635	38.358	B6 pit; in andalusite-quartz breccia
BDH121-239b	Residue	18.331	15.615	38.077	B6 pit; in andalusite-quartz breccia
BDH128-349a	Leach	19.561	15.717	38.661	Main pit; in aluminosilicate-bearing breccia
BDH128-349b	Residue	18.798	15.645	38.295	Main pit; in aluminosilicate-bearing breccia
BDH128-349c	Leach	18.813	15.644	38.276	Main pit; in aluminosilicate-bearing breccia
BDH128-349d	Residue	19.050	15.663	38.334	Main pit; in aluminosilicate-bearing breccia
BDH129-147a	Bulk	18.474	15.603	38.833	Main pit; with fine sulfides; in aluminosilicate-bearing fractured lithic breccia
BDH129-147b	Bulk	18.575	15.616	38.625	Main pit; with fine sulfides; in aluminosilicate-bearing fractured lithic breccia
BRC-3-96a	Leach	18.353	15.621	38.176	Main pit; fine- to medium-grained quartz-topaz breccia; topaz in fragments
BRC-3-96b	Residue	18.534	15.621	38.789	Main pit; fine- to medium-grained quartz-topaz breccia; topaz in fragments
BRC-3-96c	Leach	18.349	15.605	38.028	Main pit; fine- to medium-grained quartz-topaz breccia; topaz in fragments
BRC-3-96d	Residue	18.363	15.679	38.199	Main pit; fine- to medium-grained quartz-topaz breccia; topaz in fragments
Enargite					
BDH118-467a	Leach	18.535	15.625	37.250	Main pit; with pyrite and other sulfides
BDH118-467b	Residue	18.567	15.644	38.357	Main pit; with pyrite and other sulfides
BDH118-467c	Bulk	18.675	15.617	38.523	Main pit; with pyrite and other sulfides
BDH118-479	Bulk	18.596	15.613	38.217	Main pit; may include other very fine grained sulfides
BDH118-485	Bulk	18.523	15.641	38.262	Main pit; may include other very fine grained sulfides
BR2B-4a	Bulk	18.386	15.600	38.043	Main pit; topaz-altered quartz-sulfide-andalusite breccia, with rutile, zircon, minor alunite
BR2B-4b	Leach	18.301	15.596	39.117	Main pit; topaz-altered quartz-sulfide-andalusite breccia, with rutile, zircon, minor alunite
BR2B-4c	Residue	18.406	15.624	38.131	Main pit; topaz-altered quartz-sulfide-andalusite breccia, with rutile, zircon, minor alunite
Sericite					
BDH90-67a	Leach	18.495	15.661	38.091	B6 pit; with aluminosilicates and fine-grained sulfides; in quartz-pyrite-sericite schist
BDH90-67b	Residue	18.341	15.622	38.065	B6 pit; with aluminosilicates and fine-grained sulfides; in quartz-pyrite-sericite schist
BDH90-67(1)c	Leach	18.509	15.631	37.994	B6 pit; with aluminosilicates and fine-grained sulfides; in quartz-pyrite-sericite schist
BDH90-67(1)d	Residue	18.349	15.586	37.852	B6 pit; with aluminosilicates and fine-grained sulfides; in quartz-pyrite-sericite schist
BDH90-67e	Bulk	18.372	15.644	37.873	B6 pit; with aluminosilicates and fine-grained sulfides; in quartz-pyrite-sericite schist
Haile					
Galena					
DDH34-90a	Bulk	18.274	15.639	37.953	Haile pit; fine-grained cubes with medium-grained pyrite and quartz
DDH34-90b	Bulk	18.233	15.582	37.878	Haile pit; fine-grained cubes with medium-grained pyrite and quartz
DDH34-90c	Bulk	18.249	15.584	37.902	Haile pit; fine-grained cubes with medium-grained pyrite and quartz
DDH38-95	Bulk	18.314	15.582	38.043	Haile pit; with quartz and sericite
K-feldspar					
DDH47-161a	Leach	18.250	15.566	37.815	Champion pit; feldspar-quartz veinlets with fine sericite; in metavolcanic rock
DDH47-161b	Residue	18.298	15.608	37.942	Champion pit; feldspar-quartz veinlets with fine sericite; in metavolcanic rock
DDH84-176a	Leach	18.421	15.584	37.949	Snake pit; with quartz in bands; in metavolcanic rock
DDH84-176b	Residue	18.413	15.572	37.880	Snake pit; with quartz in bands; in metavolcanic rock
DDH-254-412a	Leach	20.931	15.733	41.507	Mill pit; with coarse pyrite cubes, pyrrhotite, quartz and sericite; in metavolcanic rock
DDH-254-412b	Residue	18.676	15.639	38.426	Mill pit; with coarse pyrite cubes, pyrrhotite, quartz and sericite; in metavolcanic rock
Pyrite					
HL-1a	Leach	18.583	15.659	38.497	Haile pit; massive sulfide; may include other fine sulfides
HL-1b	Residue	18.639	15.650	38.533	Haile pit; massive sulfide; may include other fine sulfides
HL-2a	Leach	18.455	15.653	38.300	Haile pit; massive sulfide; may include other fine sulfides
HL-2b	Residue	18.513	15.634	38.312	Haile pit; massive sulfide; may include other fine sulfides
HL-3a	Leach	18.673	15.662	38.751	Haile pit; massive sulfide; with quartz, and fine-grained sericite
HL-3b	Residue	19.064	15.689	39.168	Haile pit; massive sulfide; with quartz, and fine-grained sericite

APPENDIX (*Cont.*)

Sample	Split	$^{206}Pb/^{204}Pb$	$^{207}Pb/^{204}Pb$	$^{208}Pb/^{204}Pb$	Notes
HL-4	Bulk	18.648	15.637	38.625	Haile pit; massive sulfide; may include other fine sulfides
HL-5a	Leach	18.711	15.664	38.632	Red Hill pit; massive sulfide; with quartz and fine sericite
HL-5b	Residue	19.086	15.720	39.308	Red Hill pit; massive sulfide; with quartz and fine sericite
HL-7a	Leach 1	18.507	15.694	38.525	Red Hill pit; massive sulfide; with quartz and fine sericite
HL-7b	Leach 2	18.473	15.664	38.400	Red Hill pit; massive sulfide
HL-7c	Residue	18.452	15.635	38.307	Red Hill pit; massive sulfide
HL-9a	Bulk	18.402	15.651	38.193	Red Hill pit; massive sulfide
HL-9b	Bulk	18.397	15.657	38.189	Red Hill pit; massive sulfide
HL-9c	Bulk	18.410	15.680	38.258	Red Hill pit; massive sulfide
HL-9d	Bulk	18.390	15.651	38.178	Red Hill pit; massive sulfide
HL-9e	Bulk	18.388	15.636	38.131	Red Hill pit; may include other very fine sulfides
HL-9f	Bulk	18.410	15.626	38.142	Red Hill pit; may include other very fine sulfides
HL-9g	Bulk	18.686	15.690	38.515	Red Hill pit; may include other very fine sulfides
HL-9h	Bulk	18.401	15.665	38.215	Red Hill pit; may include other very fine sulfides
HL-9i	Bulk	18.390	15.647	38.156	Red Hill pit; may include other very fine sulfides
HL-9j	Bulk	18.417	15.637	38.175	Red Hill pit; may include other very fine sulfides
HL-9k	Bulk	18.378	15.638	38.126	Red Hill pit; may include other very fine sulfides
HL-9l	Bulk	18.357	15.636	38.101	Red Hill pit; may include other very fine sulfides
HL-9m	Bulk	18.391	15.652	38.186	Red Hill pit; may include other very fine sulfides
HL-9n	Bulk	18.388	15.636	38.131	Red Hill pit; may include other very fine sulfides
HL-9o	Bulk	18.396	15.653	38.178	Red Hill pit; may include other very fine sulfides
HL-9p	Bulk	18.377	15.629	38.100	Red Hill pit; may include other very fine sulfides
HL-9q	Bulk	18.338	15.612	38.028	Red Hill pit; may include other very fine sulfides
H-23a	Leach	18.743	15.680	38.696	Haile pit; massive sulfide
H-23b	Residue	18.395	15.612	38.103	Haile pit; massive sulfide
DDH34-90	Bulk	18.007	15.438	37.380	Haile pit; massive sulfide; medium- to coarse-grained pyrite (blobs), intensely silicified
DDH38-95a	Bulk	18.510	15.619	38.281	Haile pit; massive sulfide
DDH38-95b	Leach	18.635	15.631	38.512	Haile pit; massive sulfide
DDH38-95c	Residue	18.347	15.590	38.072	Haile pit; massive sulfide
H7-3272	Bulk	18.432	15.623	38.181	Red Hill pit; massive sulfide
H12-1662	Bulk	18.452	15.619	38.221	Red Hill pit; massive sulfide
H12-1662	Leach	18.461	15.618	38.228	Haile pit; massive sulfide
H12-1662	Residue	18.429	15.612	38.161	Haile pit; massive sulfide
Composite sulfides[4]					
DDH34-90a	Leach	18.633	15.608	37.989	Haile pit; massive sulfide; intensely silicified metavolcanic
DDH34-90b	Residue	18.270	15.591	37.939	Haile pit; massive sulfide; medium- to coarse-grained intensely silicified metavolcanic
DDH38-95a	Leach	18.578	15.627	38.323	Haile pit; massive sulfide; intensely silicified schist (metavolcanic)
DDH38-95b	Residue	18.691	15.609	38.491	Haile pit; massive sulfide; intensely silicified schist (metavolcanic)
DDH39-89a	Leach	18.284	15.622	38.019	Haile pit; massive sulfide; medium-grained along mid-limbs of folds; in volcaniclastic
DDH39-89b	Residue	18.307	15.654	38.113	Haile pit; massive sulfide; medium-grained along mid-limbs of folds; in volcaniclastic
DDH90-312a	Leach	18.879	15.632	39.470	Snake pit; massive sulfide; strongly foliated mudstone
DDH90-312b	Residue	20.320	15.731	39.546	Snake pit; massive sulfide; strongly foliated mudstone
DDH90-711a	Leach	18.671	15.602	38.623	Snake pit; massive sulfide; foliated, brecciated schist
DDH90-711b	Residue	19.361	15.650	39.008	Snake pit; massive sulfide; foliated, brecciated schist
DDH216-262a	Leach	18.291	15.589	38.002	Mill pit; massive sulfide; disseminated coarse to fine pyrite; in banded phyllite
DDH216-262b	Residue	18.309	15.620	38.116	Mill pit; massive sulfide; disseminated coarse to fine pyrite; in banded phyllite
Ridgeway					
Galena					
KSC126-602	Bulk	18.200	15.607	38.189	South pit; medium-grained cubes; with quartz, sericite, pyrite, molybdenite
NKF4a	Bulk	18.174	15.580	37.921	South pit; medium-grained cubes; with quartz, sericite, pyrite, molybdenite
NKF4b	Bulk	18.169	15.561	37.862	South pit; medium-grained cubes; with quartz, sericite, pyrite, molybdenite

APPENDIX (*Cont.*)

Sample	Split	$^{206}Pb/^{204}Pb$	$^{207}Pb/^{204}Pb$	$^{208}Pb/^{204}Pb$	Notes
RID(1)	Bulk	18.189	15.583	37.936	North pit; fine-grained cubes; with quartz, sericite, pyrite
RID(2)	Bulk	18.212	15.609	38.032	North pit; fine-grained cubes; with quartz, sericite, pyrite
RID(3)	Bulk	18.267	15.572	38.058	North pit; fine-grained cubes; with quartz, sericite, pyrite
RID(4)	Bulk	18.228	15.585	37.972	South pit; fine-grained cubes; with quartz, sericite, pyrite
Pyrite					
APC78-397a	Leach	18.495	15.622	38.296	North pit; coarse-grained pyrite cubes
APC78-397b	Residue	18.385	15.620	38.179	North pit; coarse-grained pyrite cubes
APD8-130a	Leach	18.296	15.593	38.133	North pit; fine-grained, disseminated pyrite cubes in streaks, in silicified siltstone (or ash)
APD8-130b	Residue	18.181	15.601	38.001	North pit; fine-grained, disseminated pyrite cubes in streaks, in silicified siltstone (or ash)
APD8-130c	Leach 1	18.323	15.580	38.193	North pit; fine-grained, disseminated pyrite cubes in streaks, in silicified siltstone (or ash)
APD8-130d	Leach 2	18.616	15.627	38.396	North pit; fine-grained, disseminated pyrite cubes in streaks, in silicified siltstone (or ash)
APD8-130e	Leach 3	19.284	15.710	38.479	North pit; fine-grained, disseminated pyrite cubes in streaks, in silicified siltstone (or ash)
APD8-130f	Residue	18.198	15.625	38.105	North pit; fine-grained, disseminated pyrite cubes in streaks, in silicified siltstone (or ash)
APD8-279a	Leach 1	18.530	15.645	38.483	North pit; fine- to coarse-grained cubic pyrite, in lenses along cleavage; with molybdenite
APD8-279b	Leach 2	18.602	15.650	38.682	North pit; fine- to coarse-grained cubic pyrite, in lenses along cleavage; with molybdenite
APD8-279c	Leach 3	18.300	15.607	38.186	North pit; fine- to coarse-grained cubic pyrite, in lenses along cleavage; with molybdenite
APD8-279d	Residue	19.352	15.693	39.190	North pit; fine- to coarse-grained cubic pyrite, in lenses along cleavage; with molybdenite
APD8-296a	Bulk	18.532	15.606	38.360	North pit; pyrite cubes with sericite and late molybdenite-quartz veins
APD8-296b	Leach 1	18.641	15.631	38.435	North pit; pyrite cubes with sericite and late molybdenite-quartz veins
APD8-296c	Leach 2	18.562	15.611	38.889	North pit; pyrite cubes with sericite and late molybdenite-quartz veins
APD8-296d	Leach 3	18.360	15.604	38.158	North pit; pyrite cubes with sericite and late molybdenite-quartz veins
APD8-296e	Residue	20.618	15.787	43.705	North pit; pyrite cubes with sericite and late molybdenite-quartz veins
APD8-300a	Leach	18.463	15.622	38.261	North pit; disseminated pyrite streaks and lenses; intensely deformed
APD8-300b	Residue	18.388	15.606	38.191	North pit; disseminated pyrite streaks and lenses; intensely deformed
APD8-300c	Leach 1	18.484	15.621	38.265	North pit; disseminated pyrite streaks and lenses; intensely deformed
APD8-300d	Leach 2	18.565	15.616	38.509	North pit; disseminated pyrite streaks and lenses; intensely deformed
APD8-300e	Leach 3	18.362	15.622	38.225	North pit; disseminated pyrite streaks and lenses; intensely deformed
APD8-300f	Residue	18.796	15.632	38.815	North pit; disseminated pyrite streaks and lenses; intensely deformed
APD8-342a	Leach 1	18.391	15.632	38.285	North pit; coarse-grained pyrite clusters in quartz veins in chlorite-sericite siltstone
APD8-342b	Leach 2	18.402	15.619	38.287	North pit; coarse-grained pyrite clusters in quartz veins in chlorite-sericite siltstone
APD8-342c	Residue	18.415	15.610	38.251	North pit; coarse-grained pyrite clusters in quartz veins in chlorite-sericite siltstone
APD8-392a	Leach	18.489	15.650	38.406	North pit; coarse-grained pyrite cubes in chlorite-sericite siltstone
APD8-392b	Residue	18.437	15.606	38.271	North pit; coarse-grained pyrite cubes in chlorite-sericite siltstone
KSC146-175a	Leach 1	18.378	15.708	38.386	South pit; fine-grained pyrite cubes, lenses, blebs; with molybdenite in chloritic siltstone
KSC146-175b	Leach 2	18.293	15.675	38.446	South pit; fine-grained pyrite cubes, lenses, blebs; with molybdenite in chloritic siltstone
KSC146-175c	Residue	18.215	15.719	38.322	South pit; fine-grained pyrite cubes, lenses, blebs; with molybdenite in chloritic siltstone
KSC146-225	Bulk	19.441	15.711	39.384	South pit; coarse-grained pyrite and molybdenite in siltstone and graywacke
KSC146-254a	Leach 1	18.317	15.645	38.202	South pit; fine-grained pyrite in silicified, veined chloritic siltstone; with molybdenite
KSC146-254b	Residue	18.284	15.719	38.373	South pit; fine-grained pyrite in silicified, veined chloritic siltstone; with molybdenite
KSC146-254c	Bulk	20.513	15.793	39.904	South pit; fine-grained pyrite in silicified, veined chloritic siltstone; with molybdenite
KSC146-267a	Leach 1	18.309	15.707	38.408	South pit; pyrite lenses in chloritic, sericitic, veined siltstone; with molybdenite
KSC146-267b	Leach 2	18.265	15.643	38.209	South pit; pyrite lenses in chloritic, sericitic, veined siltstone; with molybdenite
KSC146-267c	Leach 3	18.137	15.637	38.100	South pit; pyrite lenses in chloritic, sericitic, veined siltstone; with molybdenite
KSC146-267d	Residue	19.260	15.705	39.640	South pit; pyrite lenses in chloritic, sericitic, veined siltstone; with molybdenite
KSC146-294a	Leach 1	18.263	15.633	38.285	South pit; fine-grained pyrite in green chloritic laminated siltstone
KSC146-294b	Leach 2	18.242	15.598	38.179	South pit; fine-grained pyrite in green chloritic laminated siltstone
KSC146-294c	Residue	18.215	15.613	38.209	South pit; fine-grained pyrite in green chloritic laminated siltstone
KSC196-225a	Leach 1	18.352	15.653	38.268	South pit; chloritic siltstone with pyrite and other very fine grained sulfides
KSC196-225b	Residue	18.178	15.603	37.980	South pit; chloritic siltstone with pyrite and other very fine grained sulfides
KSC196-254	Bulk	18.159	15.580	37.940	South pit; chloritic siltstone with pyrite and other very fine grained sulfides
KSC196-294a	Leach 1	18.239	15.594	38.154	South pit; fine-grained pyrite in chloritic siltstone with quartz and fine grained sericite
KSC196-294b	Residue	18.242	15.638	38.287	South pit; fine-grained pyrite in chloritic siltstone with quartz and fine grained sericite

APPENDIX (*Cont.*)

Sample	Split	$^{206}Pb/^{204}Pb$	$^{207}Pb/^{204}Pb$	$^{208}Pb/^{204}Pb$	Notes
NKF4c	Bulk	19.113	15.709	39.290	South pit; medium- to coarse-grained pyrite with fine grained sulfides, quartz, and sericite
Molybdenite					
RID 1(1)	Leach 1	18.131	15.605	38.059	North pit; in quartz-pyrite veins, with chalcopyrite, sericite, and sphalerite
RID 1(2)	Leach 2	18.136	15.596	38.042	North pit; in quartz-pyrite veins, with chalcopyrite, sericite, and sphalerite
RID 1(3)	Leach 3	18.123	15.615	38.074	North pit; in quartz-pyrite veins, with chalcopyrite, sericite, and sphalerite
RID 1(4)	Residue	18.080	15.582	37.954	North pit; in quartz-pyrite veins, with chalcopyrite, sericite, and sphalerite
RID 2(1)	Leach 1	18.146	15.557	37.982	North pit; in veins with quartz, pyrite, chalcopyrite, and sericite
RID 2(2)	Leach 2	18.243	15.653	38.334	North pit; in veins with quartz, pyrite, chalcopyrite, and sericite
RID 2(3)	Leach 3	18.131	15.573	38.080	North pit; in veins with quartz, pyrite, chalcopyrite, and sericite
RID 2(4)	Residue	18.351	15.602	38.160	North pit; in veins with quartz, pyrite, chalcopyrite, and sericite
Chalcopyrite					
RID1 (1)	Leach 1	18.181	15.577	37.913	North pit; in veins with quartz, pyrite, sericite, sphalerite, molybdenite
RID1 (2)	Leach 2	18.205	15.608	38.013	North pit; in veins with quartz, pyrite, sericite, sphalerite, molybdenite
RID1 (3)	Leach 3	18.183	15.582	37.929	North pit; in veins with quartz, pyrite, sericite, sphalerite, molybdenite
RID1 (4)	Residue	18.216	15.618	38.043	North pit; in veins with quartz, pyrite, sericite, sphalerite, molybdenite
RID2 (2)	Leach 1	18.377	15.632	38.223	North pit; in veins with quartz, pyrite, sericite, molybdenite
RID2 (3)	Leach 2	18.371	15.618	38.171	North pit; in veins with quartz, pyrite, sericite, molybdenite
RID2 (4)	Residue	18.362	15.592	38.073	North pit; in veins with quartz, pyrite, sericite, molybdenite
Sphalerite					
RID1 (1)	Leach 1	18.760	16.030	38.523	North pit; in veins with quartz, pyrite, sericite, molybdenite
RID1 (2)	Leach 2	18.422	15.652	38.310	North pit; in veins with quartz, pyrite, sericite, molybdenite
RID1 (4)	Residue	18.523	15.710	38.689	North pit; in veins with quartz, pyrite, sericite, molybdenite
Sericite					
RID1 (1)	Leach 1	38.845	16.731	76.476	North pit; in veins with quartz, pyrite, sphalerite, molybdenite
RID1 (2)	Leach 2	35.750	16.567	90.797	North pit; in veins with quartz, pyrite, sphalerite, molybdenite
RID1 (2)	Residue	35.953	16.619	91.637	North pit; in veins with quartz, pyrite, sphalerite, molybdenite
RID2 (3)	Leach	24.825	15.917	47.829	North pit; in veins with quartz, pyrite, molybdenite
RID2 (4)	Residue	19.028	15.621	38.442	North pit; in veins with quartz, pyrite, molybdenite
Barite Hill					
Galena					
BH-1	Bulk	18.016	15.550	37.605	Massive sulfide; medium- to very coarse grained cubes
BH-2	Bulk	18.020	15.561	37.610	Massive sulfide; medium- to very coarse grained cubes
PS-201012	Bulk	18.025	15.562	37.629	Massive sulfide; medium-grained cubes; with pyrite, chalcopyrite, sphalerite
PS-301012	Bulk	18.077	15.581	37.696	Massive sulfide; medium-grained cubes; with pyrite, chalcopyrite, sphalerite
Pyrite					
GRBH-111a3	Leach	18.249	15.380	38.010	Pyrite cubes and disseminated in felsic volcanic/metasedimentary rocks
GRBH-111b3	Residue	18.221	15.589	37.852	Pyrite cubes and disseminated in felsic volcanic/metasedimentary rocks
BHD2-285.2	Bulk	18.109	15.660	37.944	Massive sulfide; pyrite and other very fine grained sulfides; with barite and quartz
BHD4-155a3	Leach	18.072	15.609	37.775	Massive sulfide
BHD4-155b3	Residue	18.294	15.645	38.015	Massive sulfide
BHD4-155c3	Bulk	18.072	15.592	37.724	Massive sulfide; may include other very fine grained sulfides
BHD5-222a3	Bulk	18.062	15.572	37.646	Massive sulfide; may include other very fine grained sulfides
BDH6-149a	Bulk	18.070	15.609	37.775	Massive sulfide; may include other very fine grained sulfides
BDH6-149b	Bulk	18.060	15.580	37.689	Massive sulfide; may include other very fine grained sulfides
BDH6-149c3	Leach	18.088	15.625	37.813	Massive sulfide; with barite
BDH6-149d3	Residue	18.078	15.596	37.727	Massive sulfide; with barite
BHD6-152a3	Leach	18.103	15.567	37.710	Massive sulfide

APPENDIX (*Cont.*)

Sample	Split	$^{206}Pb/^{204}Pb$	$^{207}Pb/^{204}Pb$	$^{208}Pb/^{204}Pb$	Notes
BHD6-152b3	Residue	18.175	15.574	37.663	Massive sulfide
BHD6-153a3	Leach	18.091	15.605	37.758	Massive sulfide
BHD6-153b3	Residue	18.112	15.628	37.832	Massive sulfide
BDH6-154a	Bulk	18.073	15.589	37.720	Massive sulfide; may include other very fine grained sulfides
BDH6-154b	Bulk	18.094	15.612	37.795	Massive sulfide; may include other very fine grained sulfides
BDH6-159a3	Leach	18.059	15.574	37.661	Massive sulfide; may include other very fine grained sulfides
BDH6-159b3	Residue	18.077	15.590	37.698	Massive sulfide
BDH6-170a3	Bulk	18.094	15.614	37.777	Massive sulfide; may include other very fine grained sulfides
BDH6-170b3	Bulk	18.089	15.622	37.807	Massive sulfide; may include other very fine grained sulfides
BDH6-189a	Bulk	18.061	15.586	37.705	Massive sulfide; may include other very fine grained sulfides
BDH6-189b	Bulk	18.079	15.601	37.743	Massive sulfide; may include other very fine grained sulfides
BHD11-171a3	Leach	18.078	15.601	37.743	Massive sulfide
BHD11-171b3	Residue	18.057	15.564	37.626	Massive sulfide
BHD11-171b3	Leach	18.096	15.603	37.751	Massive sulfide
BHD11-171d3	Residue	18.082	15.597	37.731	Massive sulfide
BHD11-171e	Leach	18.093	15.612	37.777	Massive sulfide
BHD11-171f3	Residue	18.102	15.623	37.812	Massive sulfide
BHD17-453	Bulk	18.020	15.549	37.555	Massive sulfide; may include other very fine-grained sulfides
Chalcopyrite					
BHD5-222a	Bulk	18.005	15.603	37.746	Massive sulfide; may include other very fine grained sulfides
BHD5-222b	Bulk	18.037	15.627	37.819	Massive sulfide; may include other very fine grained sulfides

Notes: Analyzed sample splits include leaches (see below), residue material after leach (Residue), and a pure bulk mineral separate (Bulk)

[1] Leaches: basic leach = 6*N* HCl, leach 1 = 1*N* HBr-1*N* HCl, leach 2 = 8*N* HBr, leach 3 = 14*N* HNO3

[2] Data from LeHuray (1982)

[3] Data from Seal et al. (2001)

[4] Composite sulfides: pyrite and other very fine grained sulfides and silicates(?)